Title
Targeting acid ceramidase inhibits YAP/TAZ signaling to reduce fibrosis in mice

Journal
Science Translational Medicine, 12(557)

ISSN
1946-6234

Authors
Alsamman, Sarah
Christenson, Stephanie A
Yu, Amy
et al.

Publication Date
2020-08-19

DOI
10.1126/scitranslmed.aay8798

Peer reviewed

HHS Public Access

Author manuscript

Sci Transl Med. Author manuscript; available in PMC 2021 March 19.

Published in final edited form as:

Sci Transl Med. 2020 August 19; 12(557): . doi:10.1126/scitranslmed.aay8798.

Targeting acid ceramidase inhibits YAP/TAZ signaling to reduce fibrosis in mice

Sarah Alsamman[1], **Stephanie A. Christenson**[2], **Amy Yu**[1], **Nadia M.E. Ayad**[3,4], **Meghan S. Mooring**[5], **Joe M. Segal**[1], **Jimmy Kuang-Hsien Hu**[6], **Johanna R. Schaub**[7], **Steve S. Ho**[7], **Vikram Rao**[7], **Megan M. Marlow**[7], **Scott M. Turner**[7], **Mai Sedki**[8], **Lorena Pantano**[9], **Sarani Ghoshal**[10], **Diego Dos Santos Ferreira**[11], **Hsiao-Yen Ma**[12], **Caroline C. Duwaerts**[1,13], **Regina Espanol-Suner**[14], **Lan Wei**[10], **Benjamin Newcomb**[15], **Izolda Mileva**[15], **Daniel Canals**[15], **Yusuf A. Hannun**[15], **Raymond T. Chung**[16], **Aras N. Mattis**[13,17], **Bryan C. Fuchs**[10], **Andrew M. Tager**[†,18], **Dean Yimlamai**[5], **Valerie M. Weaver**[3,4,14,19,20,21], **Alan C. Mullen**[16], **Dean Sheppard**[*,2,12], **Jennifer Y. Chen**[*,1,13]

[1]Department of Medicine, University of California, San Francisco, San Francisco, CA 94115, USA.

[2]Division of Pulmonary, Critical Care, Sleep & Allergy, Department of Medicine, University of California, San Francisco, San Francisco, CA 94158, USA.

[3]Center for Bioengineering and Tissue Regeneration, Department of Surgery, University of California San Francisco, San Francisco, CA 94143, USA.

[4]UC Berkeley–UCSF Graduate Program in Bioengineering, CA 94143, USA.

[5]Yale University School of Medicine, Division of Pediatric Gastroenterology and Hepatology, New Haven, CT 06520, USA.

[6]Division of Oral Biology & Medicine, School of Dentistry, University of California Los Angeles, Los Angeles, CA 90095, USA.

[7]Pliant Therapeutics, South San Francisco, CA 94080, USA.

[8]Internal Medicine, Kaiser Permanente, San Francisco, CA 94115, USA.

[9]Department of Biostatistics, Harvard School of Public Health, Boston, MA 02115, USA.

[10]Division of Surgical Oncology, Massachusetts General Hospital Cancer Center, Harvard Medical School, Boston, MA 02114, USA.

[*]To whom correspondence should be addressed. Dean.Sheppard@ucsf.edu, Jennifer.Chen4@ucsf.edu.

[†]Deceased

Author Contributions: J.Y.C., S.A., A.M.T, A.C.M, and D.S. conceived and designed the project. S.A. and A.Y. led the in vitro and mouse studies, with assistance from M.S., S.G., D.D.F, H.-Y.M., R.E.-S., L.W., and B.C.F. S.A.C. performed the computational analyses with assistance from L.P. N.M.E.A. led the studies with atomic force microscopy. J.R.S, S.S.H., V.R., M.M.M., and S.M.T. led the studies with precision cut slices. B.N., I.M., D.C., and Y.A.H. performed the sphingolipid studies and analysis. J.M.S. led the human data tissue analysis. M.S.M and D.Y. performed and analyzed the IF experiments using mouse liver tissue. A.N.M. analyzed the mouse tissue histology. J.K.-H.H, C.C.D., R.T.C., B.C.F, and V.M.W. contributed reagents and provided substantial intellectual contribution on study design. S.A., S.A.C., V.M.W., D.S., and J.Y.C. wrote the manuscript.

Competing Interests: The authors declare the following competing interests: D.S. is a founder of Pliant Therapeutics and has received research funding from Abbvie, Pfizer and Pliant Therapeutics. He serves on the Scientific Review Board for Genentech, xCella Biosciences and Optikira. J.R.S., S.S.H., V.R., M.M.M., and S.M.T. are employees of Pliant Therapeutics.

[11]The Athinoula A. Martinos Center for Biomedical Imaging, The Institute for Innovation in Imaging, Department of Radiology, Massachusetts General Hospital & Harvard Medical School, Charlestown, MA 02129, USA.

[12]Lung Biology Center, Department of Medicine, University of California, San Francisco, San Francisco, CA 94158, USA.

[13]The Liver Center, Department of Medicine, University of California, San Francisco, San Francisco, CA 94143, USA.

[14]Eli and Edythe Broad Center of Regeneration Medicine and Stem Cell Research, University of California, San Francisco, San Francisco, CA 94143, USA.

[15]Departments of Medicine and Biochemistry and the Stony Brook Cancer Center, Stony Brook University, Stony Brook, NY 11794, USA.

[16]Liver Center, Division of Gastroenterology, Department of Medicine, Massachusetts General Hospital, Boston, MA 02114, USA.

[17]Department of Pathology, University of California, San Francisco, San Francisco, CA 94143, USA.

[18]Division of Pulmonary and Critical Care Medicine, Fibrosis Research Center, and Center for Immunology and Inflammatory Diseases, Massachusetts General Hospital, Boston, MA 02114, USA.

[19]Helen Diller Family Comprehensive Cancer Center, University of California San Francisco, San Francisco, CA 94158, USA.

[20]Department of Bioengineering and Therapeutic Sciences, University of California San Francisco, San Francisco, CA 94158, USA.

[21]Department of Radiation Oncology, University of California San Francisco, San Francisco, CA 94143, USA.

Abstract

Hepatic stellate cells (HSCs) drive hepatic fibrosis. Therapies that inactivate HSCs have clinical potential as antifibrotic agents. We previously identified acid ceramidase (aCDase) as an antifibrotic target. We showed that tricyclic antidepressants (TCAs) reduce hepatic fibrosis by inhibiting aCDase and increasing the bioactive sphingolipid, ceramide. We now demonstrate that targeting aCDase inhibits YAP/TAZ activity by potentiating its phosphorylation-mediated proteasomal degradation via the ubiquitin ligase adaptor protein, β-TrCP. In mouse models of fibrosis, pharmacologic inhibition of aCDase or genetic knockout of aCDase in HSCs reduces fibrosis, stromal stiffness, and YAP/TAZ activity. In patients with advanced fibrosis, aCDase expression in HSCs is increased. Consistently, a signature of the genes most downregulated by ceramide identifies patients with advanced fibrosis who could benefit from aCDase targeting. The findings implicate ceramide as a critical regulator of YAP/TAZ signaling and HSC activation and highlight aCDase as a therapeutic target for the treatment of fibrosis.

Introduction

Fibrosis develops in response to chronic injury in nearly all organs and is characterized by progressive matrix stiffening. Tissue fibrosis is associated with high morbidity and mortality: severe fibrosis is estimated to account for almost half of all deaths in the developed world (1). Treatment options for fibrosis are limited, and organ transplantation is the only effective option for end-stage disease. There is an urgent need to understand mechanisms of fibrosis and identify new therapeutic strategies.

Activation of fibrogenic effector cells represents a key step in the pathogenesis of fibrosis. Several factors promote persistent fibroblast activation, including matrix stiffening (2-5). Central to the mechanosensing regulation of fibroblast activation are the Hippo-related transcriptional co-activators Yes-associated protein/Transcriptional coactivator with PDZ-binding motif (YAP/TAZ) (6-9). Activation of YAP/TAZ mechanosignaling promotes fibrosis in multiple organs, including the liver, kidney, skin, and lung (6, 8, 10-21). Selective targeting of YAP/TAZ in fibroblasts has been shown to attenuate fibrosis: fibroblast-selective deletion of YAP/TAZ reduced kidney fibrosis (9) and dopamine receptor D1 agonism reversed lung fibrosis (22) in mice. Strategies to interrupt the feed-forward cycle of matrix stiffness and fibroblast activation by inhibiting YAP/TAZ signaling provide an important framework to reduce fibrosis.

In this study, we identify a therapeutic strategy to promote fibroblast inactivation and reduce fibrosis. We demonstrate the sphingolipid ceramide as a potent inhibitor of YAP/TAZ signaling and show that acid ceramidase (aCDase) inhibition and deficiency in hepatic stellate cells (HSCs) reduce fibrosis in mice. Our study also highlights the therapeutic potential of aCDase targeting in patients with liver fibrosis.

Results

Ceramide regulates the Hippo signaling pathway in human hepatic stellate cells

Hepatic stellate cells (HSCs) are the primary cell type responsible for liver fibrosis (23, 24). In their quiescent state, HSCs store vitamin A in lipid droplets (25). In response to chronic injury, HSCs undergo activation, characterized by loss of lipid droplets and production of extracellular matrix (ECM) proteins. The deposition and cross-linking of ECM by activated HSCs leads to liver fibrosis and subsequent liver failure (26-28).

To identify novel antifibrotic targets, we previously performed a small molecule screen to detect compounds that promote HSC inactivation. We observed multiple screen hits in one class of compounds: tricyclic antidepressants (TCAs). We found that TCAs promote HSC inactivation by increasing the sphingolipid ceramide through inhibition of the enzyme responsible for ceramide metabolism, acid ceramidase (aCDase). We demonstrated that 25 μM ceramide-C6 inactivated HSCs, with minimal evidence of apoptosis or necrosis (29). This is consistent with other studies that demonstrated preserved viability at this dose in multiple cell types, including fibroblasts (30-32). Here, we sought to determine how ceramide promotes HSC inactivation. We analyzed RNA sequencing (RNAseq) data from culture-activated human HSCs treated with 25 μM ceramide-C6 or vehicle, and performed

Ingenuity pathway analysis (IPA) on the differentially expressed genes. IPA confirmed actin cytoskeleton signaling ($P = 1.0 \times 10^{-10}$) and HSC activation ($P = 1.21 \times 10^{-10}$) as key pathways regulated by ceramide (Fig. 1A, table S1, and data file S1).

Using gene set enrichment analysis (GSEA), we confirmed that ceramide promotes a gene expression pattern consistent with HSC inactivation after comparing the ceramide dataset with a public dataset of human activated and quiescent HSCs (33). We observed significant enrichment of genes downregulated in activated HSCs amongst those upregulated by ceramide treatment ($P = 1.27 \times 10^{-18}$) (Fig. 1, B and C). Conversely, there was significant enrichment of genes upregulated in activated HSCs amongst those downregulated by ceramide ($P = 0.006$) (Fig. 1, B and C). We similarly observed that genes up- and downregulated in reverted HSCs, as compared to activated HSCs, were enriched amongst genes up- and downregulated by ceramide treatment, respectively ($P = 5.91 \times 10^{-6}$ and 9.02×10^{-9}) (fig. S1, A and B). These findings corroborate our prior findings that ceramide inactivates human HSCs (29). Furthermore, we confirmed that ceramide promotes inactivation of culture-activated human HSCs after treatment with transforming growth factor-beta (TGF-β), a potent stimulus of fibrosis (34) (fig. S1, C and D).

Moreover, IPA revealed the Hippo pathway as a significant canonical pathway increased by ceramide ($P = 3.2 \times 10^{-7}$, Fig. 1A, table S1, and data file S1). In addition, IPA identified YAP as a significant upstream regulator of the gene expression changes inhibited by ceramide ($P = 1.0 \times 10^{-17}$), suggesting that YAP regulates these ceramide-repressed gene expression changes.

The Hippo pathway and its effectors, YAP and TAZ, have been identified as key regulators of fibrosis. Specifically, YAP was shown to drive the earliest changes in gene expression during HSC activation, and YAP inhibition leads to HSC inactivation and fibrosis reduction (10-13). We next aimed to understand the relationship between the genes regulated by ceramide and those regulated by YAP/TAZ. Using GSEA, we compared our dataset of HSCs treated with ceramide or vehicle with a public dataset of HepG2 cells transfected with siRNAs targeting YAP and TAZ in combination (35). We found significant enrichment of genes downregulated after YAP and TAZ knockdown amongst genes downregulated by ceramide treatment ($P = 6.1 \times 10^{-23}$) (Fig. 1, D and E), suggesting that ceramide mediates its transcriptional response by inhibiting YAP and TAZ. We repeated these analyses using public datasets of YAP and TAZ knockdown in HaCAT cells, observing similar findings (fig. S1, E and F). We confirmed in culture-activated human HSCs that ceramide suppresses expression of YAP/TAZ transcriptional targets, including *ANKRD1* and *CTGF* (Fig. 1F).

Ceramide promotes β-TrCP-mediated proteasomal YAP/TAZ degradation

The transcriptional activity of YAP/TAZ is influenced by their localization in the nucleus or cytoplasm, which is regulated by multiple inputs including mechanical stimuli, cell-cell contact, and G protein-coupled receptor signaling (36-38). Many of these inputs are relayed through the LATS1/2 kinase cascade, where activated phospho-LATS1/2 phosphorylate YAP/TAZ on serine residues, including serine 127 (S127 in YAP; S89 in TAZ), which promotes YAP/TAZ cytoplasmic retention, and serine 397 (S397 in YAP; S311 in TAZ), which promotes YAP/TAZ degradation (39). We next asked whether ceramide treatment

regulates YAP/TAZ localization in HSCs. Indeed, ceramide treatment for 6 hours significantly inhibited YAP/TAZ nuclear localization ($P < 0.0001$, Fig. 2, A and B). Furthermore, treatment with ceramide led to increased YAP phosphorylation at serine 397 and promoted YAP/TAZ degradation (Fig. 2C and fig. S2, A to C). Ceramide did not affect YAP phosphorylation at serine 127 (fig. S2D). The effect of ceramide on YAP/TAZ nuclear localization persisted 48 hours after treatment (fig. S2, E and F). Similarly, treatment with an aCDase inhibitor, B13, inhibited YAP/TAZ nuclear localization and promoted YAP/TAZ degradation (fig. S2, G to K). These results suggest that aCDase inhibition and ceramide accumulation promote Hippo signaling to inhibit nuclear accumulation of YAP/TAZ in HSCs.

Degradation of YAP/TAZ is regulated by several phosphorylation events. Phosphorylation of S397 in YAP (S311 in TAZ) by LATS1/2 primes for additional phosphorylation of YAP on S400 by CK1ε/δ, which generates a phosphodegron motif located in the C-terminal region of YAP/TAZ (39). This motif targets YAP/TAZ for polyubiquitination by recruiting β-TrCP, a key adaptor of SCF E3 ubiquitin ligase, which subsequently promotes proteasomal degradation (39). To determine whether ceramide treatment promotes this degradation pathway of YAP/TAZ, we transfected HSCs with siRNAs targeting *BTRC* (β-TrCP). Depletion of β-TrCP abrogated the effect of ceramide on YAP/TAZ nuclear localization and TAZ degradation (Fig. 2, D to G and fig. S3A). Similarly, treatment with a proteasome inhibitor, MG132, inhibited the effect of ceramide on YAP/TAZ nuclear localization and TAZ degradation (fig. S3, B to E). Taken together, these findings suggest that ceramide regulates YAP/TAZ localization by promoting β-TrCP-mediated proteasomal degradation.

LATS1/2 mediates ceramide regulation of YAP/TAZ localization and HSC activation

We then asked whether ceramide regulation of YAP/TAZ localization is mediated by the LATS1/2 kinases. Depletion of LATS1 and LATS2 mitigated the effect of ceramide on YAP/TAZ nuclear localization (Fig. 3A and B and fig. S3F and G). We next used a mutant allele of human *YAP*, $hYAP^{S397A}$, which cannot be phosphorylated at serine 397 and thus cannot be degraded. We nucleofected human HSCs with control *hYAP* or $hYAP^{S397A}$. In cells over-expressing the control *hYAP*, immunostaining showed that ceramide inhibited nuclear localization compared to vehicle. However, in cells expressing $hYAP^{S397A}$, the effect of ceramide on YAP/TAZ nuclear localization was attenuated (Fig. 3C and D). Furthermore, expression of $hYAP^{S397A}$ inhibited the effect of ceramide on HSC inactivation (Fig. 3E and F) and downregulation of YAP/TAZ transcriptional targets (fig. S3H and I). These studies show that constitutive activation of YAP overcomes the effect of ceramide on YAP/TAZ localization and HSC inactivation. Taken together, our findings suggest that ceramide promotes LATS1/2-mediated proteasomal degradation of YAP/TAZ to inactivate HSCs.

aCDase deficiency in HSCs reduces fibrosis development

To determine the role of aCDase in HSCs in the setting of liver fibrosis, we generated an HSC-specific aCDase-deficient mouse by crossing $Asah1^{flox/flox}$ mice with *Pdgfrb*-Cre ($Asah1^{cko}$, cACKO) mice. HSCs isolated from $Asah1^{cko}$ mice had reduced expression of *Asah1* and YAP/TAZ transcriptional targets compared to HSCs isolated from control mice

(*Asah1*$^{flox/flox}$ lacking *Pdgfrb*-Cre) (fig. S4A). To determine whether aCDase deficiency in HSCs reduces fibrosis, we used the carbon tetrachloride (CCl_4) mouse model of fibrosis (Fig. 4A). *Asah1*^{cko} mice receiving CCl_4 developed reduced fibrosis compared to control mice (Fig. 4B to D). We observed a reduction in α-smooth muscle actin (α-SMA) staining in liver tissue from CCl_4-treated *Asah1*^{cko} mice compared to control mice (fig. S4B and C), suggesting decreased HSC activation. We did not observe differences in liver toxicity or inflammation between the two groups after CCl_4 treatment (fig. S4D and E). We also observed a reduction in YAP nuclear localization in HSCs from *Asah1*^{cko} mice compared to HSCs from control mice after CCl_4 treatment (Fig. 4E and F), suggesting that HSC depletion of aCDase inhibits YAP signaling in vivo.

Activation of YAP/TAZ stimulates collagen deposition by augmenting feed-forward cycles that stiffen the ECM microenvironment (6). To further investigate the relationship between aCDase and matrix stiffness, we performed atomic force microscopy (AFM) to measure matrix stiffness along fibrotic tracts as previously described (40). We observed that the stiffness was reduced in *Asah1*^{cko} mice compared to control mice in the CCl_4 model (Fig. 4G to I). Taken together, our data showing decreased YAP nuclear localization in HSCs and reduced stiffness in *Asah1*^{cko} mice suggest that the feed-forward cycle of matrix stiffness and fibroblast activation regulated by YAP/TAZ is likely attenuated with aCDase depletion in vivo.

We next asked whether aCDase depletion in HSCs modulates fibrosis development in the context of nonalcoholic steatohepatitis (NASH). NASH was modeled by a choline-deficient, L-amino acid-defined, high-fat diet (CDAHFD), which results in steatosis, inflammation, and fibrosis (Fig. 5A) (41). In response to CDAHFD, *Asah1*^{cko} mice developed less fibrosis compared to control mice (Fig. 5B to D). *Asah1*^{cko} mice and control mice developed similar degrees of hepatic steatosis and inflammation (Fig. 5E to G). Liver to body weight ratio, serum alanine aminotransferase (ALT), and hepatic triglycerides were also similar between the two groups (Fig. 5H to J). Consistent with impaired VLDL-triglyceride secretion in the CDAHFD model, we observed decreased serum triglycerides and total cholesterol in mice fed CDAHFD compared to those fed a normal diet (ND) but no differences between the groups fed CDAHFD (fig. S5A and B). Our data demonstrate that aCDase depletion in HSCs reduces NASH-induced fibrosis without worsening of steatosis or inflammation.

Moreover, we observed increased expression of YAP/TAZ targets, *Ankrd1* and *Ctgf*, in control mice fed CDAHFD compared to *Asah1*^{cko} mice or control mice fed ND, consistent with activation of YAP/TAZ signaling in fibrosis (fig. S5C and D). Among mice fed CDAHFD, *Asah1*^{cko} mice had decreased expression of *Ankrd1* and *Ctgf* compared to control mice, further suggesting YAP/TAZ inhibition in vivo. Our studies show that targeting aCDase in HSCs reduces fibrosis in two models of fibrosis, including diet-induced NASH.

aCDase inhibition reduces fibrosis

We next aimed to determine the therapeutic potential of aCDase inhibition in fibrosis. Our previous studies demonstrated that the aCDase inhibitor B13 inactivates human HSCs (29). B13 is an analogue of ceramide, the substrate of aCDase, and has been shown to inhibit aCDase and increase ceramide (42-47). Here, we confirmed that treatment with B13 or

ceramide increased ceramide in human HSCs (fig. S6A). Treatment with B13 or ceramide also increased downstream sphingolipid metabolites, sphingosine and sphingosine 1-phosphate (S1P) (fig. S6B and C).

To determine whether aCDase inhibition reduces fibrosis development in vivo, we tested the antifibrotic effects of B13 in the CCl_4 model of fibrosis. In the CCl_4 model, mice receiving CCl_4 were concomitantly treated with B13 or B13 vehicle. As a control group for fibrosis induction, mice received olive oil (fig. S7A). Among CCl_4-treated mice, B13 treatment promoted YAP degradation and decreased fibrosis development (fig. S7B to E). B13 treatment also reduced α-SMA staining and decreased *Col1a1* expression in liver tissue (fig. S7F to H), suggesting that aCDase inhibition prevents HSC activation to reduce fibrosis development. Treatment with B13 increased total hepatic ceramide, demonstrating aCDase inhibition in vivo (fig. S7I), and increased hepatic sphingosine and S1P (fig. S7J and K). There were no differences in steatosis or inflammation between mice treated with B13 and those treated with vehicle (fig. S7L). In addition, we tested nortriptyline in a CCl_4 model of fibrosis (fig. S8A). We previously identified that nortriptyline, a TCA, inhibited aCDase and increased ceramide in human HSCs (29). Nortriptyline similarly reduced CCl_4-induced fibrosis development (fig. S8B to G).

We then asked whether aCDase inhibition regulates fibrogenesis in models where fibrosis is already established. We treated mice with CCl_4 for 6 weeks to establish fibrotic disease and then with B13 or vehicle for an additional 3 weeks of CCl_4. Mice receiving olive oil for 6 weeks and then B13 or vehicle for an additional 3 weeks of olive oil were included as controls (Fig. 6A). B13 treatment reduced liver fibrosis even after fibrotic disease was established (Fig. 6B to D). Among mice treated with CCl_4, there were no differences in liver toxicity, steatosis, or inflammation between mice receiving B13 or vehicle (fig. S9A to D).

Next, we measured whether aCDase inhibition reduces fibrogenesis using precision cut liver slices (PCLS) from both rats and humans. PCLS are viable explants containing all types of liver cells in their natural environment, and have been used as an ex vivo method to study drug metabolism, toxicity, and fibrogenesis (48-52). We prepared PCLS from rats fed CDAHFD and treated the fibrotic slices with aCDase inhibitors for 48 hours (Fig. 6E). Rats fed CDAHFD for 18 weeks developed fibrosis as evidenced by picrosirus red staining (fig. S9E). B13 treatment reduced expression of profibrotic genes, including *Acta2, Col1a1*, and *Col1a2* (Fig. 6F). Similarly, Ceranib 1, another aCDase inhibitor (53), led to a dose-dependent reduction in profibrotic gene expression (Fig. 6G). Viability of the PCLS was confirmed at 48 hours (fig. S9F and G). Our data demonstrate that aCDase inhibition reduces fibrogenesis in the setting of established NASH fibrosis ex vivo.

Furthermore, we prepared PCLS from the livers of 2 patients undergoing liver transplantation (1 with alcoholic cirrhosis and 1 with primary biliary cirrhosis, PBC) (Fig. 6H). Consistent with the rat data, we observed that Ceranib 1 reduced expression of profibrotic genes (Fig. 6I). These data suggest that aCDase inhibition reduces established liver fibrosis in tissue from rats and humans with multiple etiologies of liver disease (NASH, alcohol, and PBC).

aCDase and the ceramide responsiveness score are increased in patients with advanced liver fibrosis

Given our findings that ceramide regulates the Hippo pathway to promote YAP/TAZ cytoplasmic localization and degradation, inhibit HSC activation, and reduce fibrosis, we asked whether these pathways are dysregulated in patients with advanced hepatic fibrosis. Staining of liver sections from patients with chronic hepatitis C virus infection (HCV) and advanced fibrosis showed increased aCDase expression in HSCs compared to those with no fibrosis (Fig. 7A and B). In addition, we did not observe aCDase staining in hepatocytes.

Next, we determined whether the expression of the 100 genes most downregulated by ceramide in our experiments were altered by fibrosis severity in patients with nonalcoholic fatty liver disease (NAFLD). We examined a public dataset of 72 patients with NAFLD, of whom 40 had mild fibrosis (stage 0-1) and 32 had advanced fibrosis (stage 3-4) (54). Using GSEA, we found significant enrichment of genes downregulated by ceramide amongst those upregulated in advanced fibrosis ($P = 0.00002$) (Fig. 7C). We used gene set variation analysis (GSVA) to then generate a gene set enrichment score on a per-patient basis of these 100 ceramide-downregulated genes (the “ceramide responsiveness score”) (data file S2). The ceramide responsiveness score was 1.2 log fold higher in patients with NAFLD and advanced fibrosis as compared to those with mild fibrosis ($P < 0.0001$) (Fig. 7D).

We also generated enrichment score metrics in the NAFLD dataset for gene sets of ceramide-responsive genes in the YAP and HSC activation pathways as these are the biological pathways of greatest interest. The genes included for each pathway were those genes that were differentially expressed in response to ceramide and identified by IPA to be associated with each biological function (data file S2). A heatmap shows that all metrics, including the ceramide responsiveness score, were coordinately upregulated in patients with advanced fibrosis (Fig. 7E). These data show that the biological pathways of interest (YAP, HSC activation) are upregulated in association with advanced fibrosis, corroborating their importance in fibrosis progression. Moreover, the coordinately upregulated expression of the ceramide responsiveness score suggests that the transcriptional response associated with increasing fibrosis could be reversed with aCDase inhibition.

Discussion

Fibrosis is a pathological feature of disease in virtually all organs, and accounts for considerable morbidity and mortality. In patients with organ fibrosis, a feed forward cycle of matrix stiffness, fibroblast activation and proliferation, and matrix accumulation perpetuates fibrosis progression (2). YAP/TAZ mechanosignaling promotes fibrosis in multiple organs, including the liver, kidney, skin, and lung (6, 8, 10-20), suggesting its relevance as a core pathway. In this study, we uncovered a signaling network through which aCDase inhibition regulates phosphorylation and degradation of YAP/TAZ. Pharmacologic inhibition or genetic knockout of aCDase in HSCs attenuated fibrosis in mice, and targeting aCDase reduced fibrogenesis in the setting of established fibrosis. This work highlights aCDase inhibition as a potential therapeutic strategy for the treatment of hepatic fibrosis. We also demonstrated that targets of ceramide- and YAP/TAZ signaling have the potential to serve as markers of fibrosis.

The Hippo-YAP/TAZ network plays an important role in regulating organ size, regeneration, and cell fate (55-59). In the liver, the regulation and biological functions of YAP/TAZ signaling are complex and cell type specific (60). YAP drives HSC activation, and inhibition of YAP by verteporfin reduced HSC activation and fibrogenesis (10-12). In hepatocytes, YAP/TAZ activity is increased in chronic liver injury and deletion of YAP/TAZ attenuated liver inflammation and fibrosis (61). TAZ expression is increased in mouse and human NASH, and silencing of hepatocyte TAZ ameliorated NASH fibrosis (62). YAP/TAZ hyperactivation promotes tumorigenesis in the liver (63, 64) and correlates with poor prognosis (65-67). However, YAP/TAZ activation in peritumoral hepatocytes has been shown to exert a tumor-suppressive function (68). Furthermore, YAP is essential for adult biliary cell survival under homeostatic conditions and is required in hepatocytes for the ductular response during regeneration (69, 70). The diversity of functions mediated by YAP/TAZ within and between different cell types highlights the need for cell-specific approaches to inhibit their pathologic functions in liver disease. Additionally, the redundancy in the roles of YAP and TAZ remains to be fully elucidated.

Our studies demonstrate increased aCDase expression in activated HSCs in patients with advanced fibrosis, with little aCDase expression in other cell types of the liver including hepatocytes. This suggests that targeting aCDase may represent a fibroblast-specific approach to inhibit YAP/TAZ signaling and reduce fibrosis, with potentially minimal effects on hepatocytes in vivo. Additional studies are needed to elucidate the factors that promote aCDase activity in HSCs and assess the effects of targeting aCDase on YAP/TAZ in other cell types of the liver.

Our work illustrates the potential clinical relevance of aCDase inhibition and ceramide accumulation in reducing fibrosis. Studies have suggested that ceramide promotes insulin resistance to increase hepatic steatosis (71-74). Ceramide accumulation in the liver and plasma correlates with insulin resistance and hepatic steatosis (75-80), and inducible overexpression of aCDase in hepatocytes prevented hepatic steatosis in mice receiving a high-fat diet (73). However, in our studies deletion of aCDase in HSCs reduced fibrosis in a mouse model of NASH and did not worsen steatosis or lobular inflammation. Similarly, we did not observe increased steatosis or lobular inflammation in *Asah1*^{cko} mice or mice treated with the aCDase inhibitor B13 compared to their respective controls. ACDase inhibition reduced active fibrogenesis in NASH fibrotic liver slices from rats. Furthermore, we demonstrated in patients with NAFLD that genes downregulated by ceramide treatment in HSCs were enriched amongst genes upregulated in patients with advanced compared to mild fibrosis. This suggests that ceramide could ameliorate fibrosis-induced gene expression changes in the context of NAFLD. Taken together, this suggests that targeting aCDase may be beneficial in reducing fibrosis without worsening other aspects of NASH. This is particularly relevant for patients, since fibrosis is the histologic feature associated with long-term progression of NASH (81).

Our previous studies highlighted the role of aCDase and ceramide in HSC activation (29). ACDase is an enzyme in the lysosomal sphingolipid degradative pathway, in which sphingomyelin and cerebrosides are first converted to ceramide through the actions of acid sphingomyelinase and acid cerebrosidase, respectively. Ceramide is then hydrolyzed by

aCDase to sphingosine, which is then able to escape the lysosome where it can be phosphorylated by sphingosine kinases 1 and 2, resulting in S1P. The sphingolipid S1P promotes YAP/TAZ nuclear localization (38) and HSC activation (82-84), contrary to the effects of ceramide observed in our studies. We sought to determine how S1P is modulated by ceramide treatment and aCDase inhibition. In HSCs, we observed that ceramide or B13 treatment increased total ceramide, sphingosine, and S1P. Similarly, treatment with B13 increased hepatic ceramide, sphingosine, and S1P in mice. Our data thus suggest that the antifibrotic effect of aCDase inhibition is mediated by ceramide rather than by a decreases in S1P. Additional studies to examine alterations in the other axes of sphingolipid metabolism (*de novo* pathway or salvage pathway) and changes in specific ceramide species are warranted in the context of targeting aCDase.

We developed a gene signature score, the ceramide responsiveness score, which correlates with advanced fibrosis. The ceramide responsiveness score may serve as a potential biomarker to identify patients with a higher fibrotic burden of disease and those who would benefit from aCDase inhibition. Similarly, the YAP score and HSC activation score could serve as biomarkers and warrant further investigation. Integration of these scores in clinical practice could facilitate a precision medicine-based approach to the treatment of fibrosis.

This study has several limitations. Our mechanistic studies involving human HSCs were limited by the difference in stability of YAP and TAZ (12, 85, 86). Our data suggest that ceramide inhibits nuclear localization of YAP/TAZ by promoting LATS1/2-mediated proteasomal degradation. Consistently, in the presence of siRNAs targeting β-TrCP or a proteasome inhibitor, the effect of ceramide on TAZ degradation was attenuated. However, the slower time course of the effects of ceramide on YAP prevented us from demonstrating similar findings because of the effects of β-TrCP depletion or proteasome inhibition on cell viability over a longer time course. We acknowledge that additional studies are needed to decipher the relationship between targeting aCDase and YAP/TAZ activity on fibroblast activation, collagen deposition, and matrix stiffness in vivo. These studies include manipulation of matrix stiffness and YAP/TAZ activity in *Asah1*^{cko} mice, and will be pursued in future analyses. Regardless, the reduction of tissue stiffness we observed provides compelling evidence that inhibition of aCDase may interrupt the previously characterized feed-forward cycle involving YAP/TAZ activation, HSC activation, and matrix stiffness. We also acknowledge that additional studies using different models of NASH are necessary to characterize the effects of targeting aCDase in vivo. Although CDAHFD-fed mice develop steatosis, inflammation, and fibrosis, they do not display several features of metabolic syndrome such as hypercholesterolemia, hypertriglyceridemia, and hyperglycemia. Finally, to proceed with clinical development of aCDase inhibitors, pharmacokinetic and pharmacodynamic studies of candidate inhibitors will be required. It will also be important to determine the impact of targeting aCDase for the treatment of fibrosis in other organs, including the lung, kidney, and skin.

In summary, our studies highlight the role of aCDase inhibition in reducing fibrosis. Further elucidation of upstream and downstream components of the ceramide and YAP/TAZ pathway may provide additional strategies to halt fibrosis progression.

Materials and Methods

Study design

The goals of this study were threefold: to identify how aCDase inhibition promotes inactivation of HSCs; to determine whether targeting aCDase ameliorates fibrosis in vivo; and to identify the clinical relevance of this pathway in patients with hepatic fibrosis. RNA sequencing and gene set enrichment analyses identified the Hippo/YAP signaling pathway as a key pathway regulated by ceramide. This led to the main hypothesis that ceramide regulates YAP/TAZ signaling to inactivate HSCs and reduce fibrosis. In cell-based assays, we treated human HSCs with ceramide and observed a profound shift in the nuclear localization of YAP/TAZ. For in vivo mouse studies, carbon tetrachloride and CDAHFD models were chosen as well-established and relevant models of liver fibrosis. Sample sizes were calculated by power analysis based on prior experience and feasibility, and a minimum of 6 mice were included in each group. Mice were randomly assigned to treatment groups. Biochemical and histological outcomes were analyzed with the investigator blinded to the treatment received. No animals were excluded as outliers from the reported dataset. All in vitro and in vivo experiments were performed in two to four technical replicates, and the number of biologically independent samples is identified in each figure. Detailed methods for the computational analyses, in vitro studies, and tissue analyses are provided in the Supplemental Materials.

Animal experiments

Animal experiments were approved by the Institutional Animal Care and Use Committee at Massachusetts General Hospital, University of California, San Francisco, and Pliant Therapeutics. All animals received humane care according to the criteria outlined in the *Guide for the Care and Use of Laboratory Animals of the National Academy of Sciences*.

For the therapeutic B13 experiment, male C57BL/6J mice (age 6 weeks, Jackson Laboratory, Bar Harbor, ME) received 0.1cc of a 6.66 percent solution of CCl_4 (Sigma) in olive oil or olive oil alone by IP 3 days/week for 9 weeks. Mice were concomitantly treated with 50 mg/kg B13 or vehicle 5 days/week by IP for the last 3 weeks of olive oil or CCl_4 treatment.

To generate the HSC depletion of aCDase, we crossed *Asah1*$^{flox/flox}$ (provided by Lina Obeid) (87) with *Pdgfrb*-Cre (88) (*Asah1*^{cko}, cACKO). Control mice were *Asah1*$^{flox/flox}$ lacking *Pdgfrb*-Cre. In the CCl_4 model, 6- to 8-week old sex-matched control and cACKO mice were treated with 0.1 cc of a 6.66 percent solution of CCl_4 (Sigma) in olive oil or olive oil alone by IP 3 times a week for 6 weeks. In the CDAHFD model, 6- to 8-week old sex-matched mice received either normal chow (PicoLab Rodent Diet 20; LabDiet #5053) or CDAHFD (L-amino acid diet with 60 kcal% fat with 0.1% methionine without added choline; Research Diets A06071302) *ad libitum* for 14 weeks.

All animals were anesthetized and sedated at the time of sacrifice. A terminal blood collection was performed by cardiac puncture. Livers were weighed, and were subsequently fixed in formalin or 4% paraformaldehyde or snap frozen for further analysis. HSC isolation was performed using the Mederacke protocol (89).

Statistics

All data are represented as the mean of at least 3 independent experiments ± s.e.m. Statistical analysis was performed using GraphPad Prism 8 with unpaired two-sided student t-tests, one-way ANOVA with Tukey's method for multiple comparisons, or Kruskal-Wallis test with Dunn's multiple comparisons test. CAMERA was used for GSEA. Statistical significance was defined as $P < 0.05$. All experiments were repeated a minimum of three times, unless otherwise stated.

Data and Materials Availability:

All data associated with this study are present within the main text or the Supplementary Materials. RNA-seq data analyzed for this study are available at GSE78853.

Supplementary Material

Refer to Web version on PubMed Central for supplementary material.

Acknowledgments:

L. Obeid (Stonybrook Cancer Center) provided *Asah1*$^{flox/flox}$ mice, and R. H. Adams (Max Planck Institute) contributed *Pdgfrb*-Cre mice to D.S. We gratefully acknowledge the core services provided by the UCSF Liver Center P30DK026743, and thank C. Her for expert technical assistance.

Funding: Research reported in this publication was supported by the National Institute of Diabetes and Digestive and Kidney Diseases of the National Institutes of Health under Award Number K08DK114548 (to J.Y.C) and the UCSF Liver Center P30DK026743 (UCSF Liver Center Pilot/Feasibility grant to J.Y.C.). The content is solely the responsibility of the authors and does not necessarily represent the official views of the National Institutes of Health. This work was also supported by funds from the UCSF Department of Medicine (to J.Y.C.).

References

1. Wynn TA, Fibrotic disease and the T(H)1/T(H)2 paradigm. Nat Rev Immunol 4, 583–594 (2004). [PubMed: 15286725]
2. Liu F, Mih JD, Shea BS, Kho AT, Sharif AS, Tager AM, Tschumperlin DJ, Feedback amplification of fibrosis through matrix stiffening and COX-2 suppression. J Cell Biol 190, 693–706 (2010). [PubMed: 20733059]
3. Arora PD, Narani N, McCulloch CA, The compliance of collagen gels regulates transforming growth factor-beta induction of alpha-smooth muscle actin in fibroblasts. Am J Pathol 154, 871–882 (1999). [PubMed: 10079265]
4. Li Z, Dranoff JA, Chan EP, Uemura M, Sevigny J, Wells RG, Transforming growth factor-beta and substrate stiffness regulate portal fibroblast activation in culture. Hepatology 46, 1246–1256 (2007). [PubMed: 17625791]
5. Georges PC, Hui JJ, Gombos Z, McCormick ME, Wang AY, Uemura M, Mick R, Janmey PA, Furth EE, Wells RG, Increased stiffness of the rat liver precedes matrix deposition: implications for fibrosis. Am J Physiol Gastrointest Liver Physiol 293, G1147–1154 (2007). [PubMed: 17932231]
6. Liu F, Lagares D, Choi KM, Stopfer L, Marinkovic A, Vrbanac V, Probst CK, Hiemer SE, Sisson TH, Horowitz JC, Rosas IO, Fredenburgh LE, Feghali-Bostwick C, Varelas X, Tager AM, Tschumperlin DJ, Mechanosignaling through YAP and TAZ drives fibroblast activation and fibrosis. Am J Physiol Lung Cell Mol Physiol 308, L344–357 (2015). [PubMed: 25502501]
7. Caliari SR, Perepelyuk M, Cosgrove BD, Tsai SJ, Lee GY, Mauck RL, Wells RG, Burdick JA, Stiffening hydrogels for investigating the dynamics of hepatic stellate cell mechanotransduction during myofibroblast activation. Sci Rep 6, 21387 (2016). [PubMed: 26906177]

8. Szeto SG, Narimatsu M, Lu M, He X, Sidiqi AM, Tolosa MF, Chan L, De Freitas K, Bialik JF, Majumder S, Boo S, Hinz B, Dan Q, Advani A, John R, Wrana JL, Kapus A, Yuen DA, YAP/TAZ Are Mechanoregulators of TGF-beta-Smad Signaling and Renal Fibrogenesis. J Am Soc Nephrol 27, 3117–3128 (2016). [PubMed: 26961347]

9. Liang M, Yu M, Xia R, Song K, Wang J, Luo J, Chen G, Cheng J, Yap/Taz Deletion in Gli(+) Cell-Derived Myofibroblasts Attenuates Fibrosis. J Am Soc Nephrol 28, 3278–3290 (2017). [PubMed: 28768710]

10. Martin K, Pritchett J, Llewellyn J, Mullan AF, Athwal VS, Dobie R, Harvey E, Zeef L, Farrow S, Streuli C, Henderson NC, Friedman SL, Hanley NA, Piper Hanley K, PAK proteins and YAP-1 signalling downstream of integrin beta-1 in myofibroblasts promote liver fibrosis. Nat Commun 7, 12502 (2016). [PubMed: 27535340]

11. Mannaerts I, Leite SB, Verhulst S, Claerhout S, Eysackers N, Thoen LF, Hoorens A, Reynaert H, Halder G, van Grunsven LA, The Hippo pathway effector YAP controls mouse hepatic stellate cell activation. J Hepatol 63, 679–688 (2015). [PubMed: 25908270]

12. Zhang K, Chang Y, Shi Z, Han X, Han Y, Yao Q, Hu Z, Cui H, Zheng L, Han T, Hong W, omega-3 PUFAs ameliorate liver fibrosis and inhibit hepatic stellate cells proliferation and activation by promoting YAP/TAZ degradation. Sci Rep 6, 30029 (2016). [PubMed: 27435808]

13. Swiderska-Syn M, Xie G, Michelotti GA, Jewell ML, Premont RT, Syn WK, Diehl AM, Hedgehog regulates yes-associated protein 1 in regenerating mouse liver. Hepatology 64, 232–244 (2016). [PubMed: 26970079]

14. Seo E, Kim WY, Hur J, Kim H, Nam SA, Choi A, Kim YM, Park SH, Chung C, Kim J, Min S, Myung SJ, Lim DS, Kim YK, The Hippo-Salvador signaling pathway regulates renal tubulointerstitial fibrosis. Sci Rep 6, 31931 (2016). [PubMed: 27550469]

15. Xu J, Li PX, Wu J, Gao YJ, Yin MX, Lin Y, Yang M, Chen DP, Sun HP, Liu ZB, Gu XC, Huang HL, Fu LL, Hu HM, He LL, Wu WQ, Fei ZL, Ji HB, Zhang L, Mei CL, Involvement of the Hippo pathway in regeneration and fibrogenesis after ischaemic acute kidney injury: YAP is the key effector. Clin Sci (Lond) 130, 349–363 (2016). [PubMed: 26574480]

16. Anorga S, Overstreet JM, Falke LL, Tang J, Goldschmeding RG, Higgins PJ, Samarakoon R, Deregulation of Hippo-TAZ pathway during renal injury confers a fibrotic maladaptive phenotype. FASEB J 32, 2644–2657 (2018). [PubMed: 29298862]

17. Schlegelmilch K, Mohseni M, Kirak O, Pruszak J, Rodriguez JR, Zhou D, Kreger BT, Vasioukhin V, Avruch J, Brummelkamp TR, Camargo FD, Yap1 acts downstream of alpha-catenin to control epidermal proliferation. Cell 144, 782–795 (2011). [PubMed: 21376238]

18. Lee MJ, Byun MR, Furutani-Seiki M, Hong JH, Jung HS, YAP and TAZ regulate skin wound healing. J Invest Dermatol 134, 518–525 (2014). [PubMed: 24108406]

19. Noguchi S, Saito A, Mikami Y, Urushiyama H, Horie M, Matsuzaki H, Takeshima H, Makita K, Miyashita N, Mitani A, Jo T, Yamauchi Y, Terasaki Y, Nagase T, TAZ contributes to pulmonary fibrosis by activating profibrotic functions of lung fibroblasts. Sci Rep 7, 42595 (2017). [PubMed: 28195168]

20. Jorgenson AJ, Choi KM, Sicard D, Smith KM, Hiemer SE, Varelas X, Tschumperlin DJ, TAZ activation drives fibroblast spheroid growth, expression of profibrotic paracrine signals, and context-dependent ECM gene expression. Am J Physiol Cell Physiol 312, C277–C285 (2017). [PubMed: 27881410]

21. Bertero T, Cottrill KA, Annis S, Bhat B, Gochuico BR, Osorio JC, Rosas I, Haley KJ, Corey KE, Chung RT, Nelson Chau B, Chan SY, A YAP/TAZ-miR-130/301 molecular circuit exerts systems-level control of fibrosis in a network of human diseases and physiologic conditions. Sci Rep 5, 18277 (2015). [PubMed: 26667495]

22. Haak AJ, Kostallari E, Sicard D, Ligresti G, Choi KM, Caporarello N, Jones DL, Tan Q, Meridew J, Diaz Espinosa AM, Aravamudhan A, Maiers JL, Britt RD Jr., Roden AC, Pabelick CM, Prakash YS, Nouraie SM, Li X, Zhang Y, Kass DJ, Lagares D, Tager AM, Varelas X, Shah VH, Tschumperlin DJ, Selective YAP/TAZ inhibition in fibroblasts via dopamine receptor D1 agonism reverses fibrosis. Sci Transl Med 11, 516 (2019).

23. Mederacke I, Hsu CC, Troeger JS, Huebener P, Mu X, Dapito DH, Pradere JP, Schwabe RF, Fate tracing reveals hepatic stellate cells as dominant contributors to liver fibrosis independent of its aetiology. Nat Commun 4, 2823 (2013). [PubMed: 24264436]

24. Friedman SL, Roll FJ, Boyles J, Bissell DM, Hepatic lipocytes: the principal collagen-producing cells of normal rat liver. Proc Natl Acad Sci U S A 82, 8681–8685 (1985). [PubMed: 3909149]
25. Wake K, "Sternzellen" in the liver: perisinusoidal cells with special reference to storage of vitamin A. Am J Anat 132, 429–462 (1971). [PubMed: 4942297]
26. Rockey DC, Weisiger RA, Endothelin induced contractility of stellate cells from normal and cirrhotic rat liver: implications for regulation of portal pressure and resistance. Hepatology 24, 233–240 (1996). [PubMed: 8707268]
27. Ballardini G, Fallani M, Biagini G, Bianchi FB, Pisi E, Desmin and actin in the identification of Ito cells and in monitoring their evolution to myofibroblasts in experimental liver fibrosis. Virchows Arch B Cell Pathol Incl Mol Pathol 56, 45–49 (1988). [PubMed: 2907200]
28. Perepelyuk M, Terajima M, Wang AY, Georges PC, Janmey PA, Yamauchi M, Wells RG, Hepatic stellate cells and portal fibroblasts are the major cellular sources of collagens and lysyl oxidases in normal liver and early after injury. Am J Physiol Gastrointest Liver Physiol 304, G605–614 (2013). [PubMed: 23328207]
29. Chen JY, Newcomb B, Zhou C, Pondick JV, Ghoshal S, York SR, Motola DL, Coant N, Yi JK, Mao C, Tanabe KK, Bronova I, Berdyshev EV, Fuchs BC, Hannun Y, Chung RT, Mullen AC, Tricyclic Antidepressants Promote Ceramide Accumulation to Regulate Collagen Production in Human Hepatic Stellate Cells. Sci Rep 7, 44867 (2017). [PubMed: 28322247]
30. Ji C, Yang B, Yang YL, He SH, Miao DS, He L, Bi ZG, Exogenous cell-permeable C6 ceramide sensitizes multiple cancer cell lines to Doxorubicin-induced apoptosis by promoting AMPK activation and mTORC1 inhibition. Oncogene 29, 6557–6568 (2010). [PubMed: 20802518]
31. Sakamoto W, Coant N, Canals D, Obeid LM, Hannun YA, Functions of neutral ceramidase in the Golgi apparatus. J Lipid Res 59, 2116–2125 (2018). [PubMed: 30154232]
32. Li R, Blanchette-Mackie EJ, Ladisch S, Induction of endocytic vesicles by exogenous C(6)-ceramide. J Biol Chem 274, 21121–21127 (1999). [PubMed: 10409665]
33. El Taghdouini A, Najimi M, Sancho-Bru P, Sokal E, van Grunsven LA, In vitro reversion of activated primary human hepatic stellate cells. Fibrogenesis Tissue Repair 8, 14 (2015). [PubMed: 26251672]
34. Dooley S, Delvoux B, Lahme B, Mangasser-Stephan K, Gressner AM, Modulation of transforming growth factor beta response and signaling during transdifferentiation of rat hepatic stellate cells to myofibroblasts. Hepatology 31, 1094–1106 (2000). [PubMed: 10796885]
35. Mori M, Triboulet R, Mohseni M, Schlegelmilch K, Shrestha K, Camargo FD, Gregory RI, Hippo signaling regulates microprocessor and links cell-density-dependent miRNA biogenesis to cancer. Cell 156, 893–906 (2014). [PubMed: 24581491]
36. Dupont S, Morsut L, Aragona M, Enzo E, Giulitti S, Cordenonsi M, Zanconato F, Le Digabel J, Forcato M, Bicciato S, Elvassore N, Piccolo S, Role of YAP/TAZ in mechanotransduction. Nature 474, 179–183 (2011). [PubMed: 21654799]
37. Zhao B, Wei X, Li W, Udan RS, Yang Q, Kim J, Xie J, Ikenoue T, Yu J, Li L, Zheng P, Ye K, Chinnaiyan A, Halder G, Lai ZC, Guan KL, Inactivation of YAP oncoprotein by the Hippo pathway is involved in cell contact inhibition and tissue growth control. Genes Dev 21, 2747–2761 (2007). [PubMed: 17974916]
38. Yu FX, Zhao B, Panupinthu N, Jewell JL, Lian I, Wang LH, Zhao J, Yuan H, Tumaneng K, Li H, Fu XD, Mills GB, Guan KL, Regulation of the Hippo-YAP pathway by G-protein-coupled receptor signaling. Cell 150, 780–791 (2012). [PubMed: 22863277]
39. Zhao B, Li L, Tumaneng K, Wang CY, Guan KL, A coordinated phosphorylation by Lats and CK1 regulates YAP stability through SCF(beta-TRCP). Genes Dev 24, 72–85 (2010). [PubMed: 20048001]
40. Desai SS, Tung JC, Zhou VX, Grenert JP, Malato Y, Rezvani M, Espanol-Suner R, Willenbring H, Weaver VM, Chang TT, Physiological ranges of matrix rigidity modulate primary mouse hepatocyte function in part through hepatocyte nuclear factor 4 alpha. Hepatology 64, 261–275 (2016). [PubMed: 26755329]
41. Matsumoto M, Hada N, Sakamaki Y, Uno A, Shiga T, Tanaka C, Ito T, Katsume A, Sudoh M, An improved mouse model that rapidly develops fibrosis in non-alcoholic steatohepatitis. Int J Exp Pathol 94, 93–103 (2013). [PubMed: 23305254]

42. Bielawska A, Linardic CM, Hannun YA, Ceramide-mediated biology. Determination of structural and stereospecific requirements through the use of N-acyl-phenylaminoalcohol analogs. J Biol Chem 267, 18493–18497 (1992). [PubMed: 1526986]
43. Raisova M, Goltz G, Bektas M, Bielawska A, Riebeling C, Hossini AM, Eberle J, Hannun YA, Orfanos CE, Geilen CC, Bcl-2 overexpression prevents apoptosis induced by ceramidase inhibitors in malignant melanoma and HaCaT keratinocytes. FEBS Lett 516, 47–52 (2002). [PubMed: 11959101]
44. Bielawska A, Bielawski J, Szulc ZM, Mayroo N, Liu X, Bai A, Elojeimy S, Rembiesa B, Pierce J, Norris JS, Hannun YA, Novel analogs of D-e-MAPP and B13. Part 2: signature effects on bioactive sphingolipids. Bioorg Med Chem 16, 1032–1045 (2008). [PubMed: 17881234]
45. Bai A, Szulc ZM, Bielawski J, Pierce JS, Rembiesa B, Terzieva S, Mao C, Xu R, Wu B, Clarke CJ, Newcomb B, Liu X, Norris J, Hannun YA, Bielawska A, Targeting (cellular) lysosomal acid ceramidase by B13: design, synthesis and evaluation of novel DMG-B13 ester prodrugs. Bioorg Med Chem 22, 6933–6944 (2014). [PubMed: 25456083]
46. Selzner M, Bielawska A, Morse MA, Rudiger HA, Sindram D, Hannun YA, Clavien PA, Induction of apoptotic cell death and prevention of tumor growth by ceramide analogues in metastatic human colon cancer. Cancer Res 61, 1233–1240 (2001). [PubMed: 11221856]
47. Samsel L, Zaidel G, Drumgoole HM, Jelovac D, Drachenberg C, Rhee JG, Brodie AM, Bielawska A, Smyth MJ, The ceramide analog, B13, induces apoptosis in prostate cancer cell lines and inhibits tumor growth in prostate cancer xenografts. Prostate 58, 382–393 (2004). [PubMed: 14968439]
48. de Graaf IA, Olinga P, de Jager MH, Merema MT, de Kanter R, van de Kerkhof EG, Groothuis GM, Preparation and incubation of precision-cut liver and intestinal slices for application in drug metabolism and toxicity studies. Nat Protoc 5, 1540–1551 (2010). [PubMed: 20725069]
49. Palma E, Doornebal EJ, Chokshi S, Precision-cut liver slices: a versatile tool to advance liver research. Hepatol Int 13, 51–57 (2019). [PubMed: 30515676]
50. Olinga P, Elferink MG, Draaisma AL, Merema MT, Castell JV, Perez G, Groothuis GM, Coordinated induction of drug transporters and phase I and II metabolism in human liver slices. Eur J Pharm Sci 33, 380–389 (2008). [PubMed: 18328680]
51. van de Bovenkamp M, Groothuis GM, Meijer DK, Olinga P, Liver slices as a model to study fibrogenesis and test the effects of anti-fibrotic drugs on fibrogenic cells in human liver. Toxicol In Vitro 22, 771–778 (2008). [PubMed: 18207697]
52. Olinga P, Schuppan D, Precision-cut liver slices: a tool to model the liver ex vivo. J Hepatol 58, 1252–1253 (2013). [PubMed: 23336979]
53. Draper JM, Xia Z, Smith RA, Zhuang Y, Wang W, Smith CD, Discovery and evaluation of inhibitors of human ceramidase. Mol Cancer Ther 10, 2052–2061 (2011). [PubMed: 21885864]
54. Moylan CA, Pang H, Dellinger A, Suzuki A, Garrett ME, Guy CD, Murphy SK, Ashley-Koch AE, Choi SS, Michelotti GA, Hampton DD, Chen Y, Tillmann HL, Hauser MA, Abdelmalek MF, Diehl AM, Hepatic gene expression profiles differentiate presymptomatic patients with mild versus severe nonalcoholic fatty liver disease. Hepatology 59, 471–482 (2014). [PubMed: 23913408]
55. Camargo FD, Gokhale S, Johnnidis JB, Fu D, Bell GW, Jaenisch R, Brummelkamp TR, YAP1 increases organ size and expands undifferentiated progenitor cells. Curr Biol 17, 2054–2060 (2007). [PubMed: 17980593]
56. Zhou D, Conrad C, Xia F, Park JS, Payer B, Yin Y, Lauwers GY, Thasler W, Lee JT, Avruch J, Bardeesy N, Mst1 and Mst2 maintain hepatocyte quiescence and suppress hepatocellular carcinoma development through inactivation of the Yap1 oncogene. Cancer Cell 16, 425–438 (2009). [PubMed: 19878874]
57. Benhamouche S, Curto M, Saotome I, Gladden AB, Liu CH, Giovannini M, McClatchey AI, Nf2/Merlin controls progenitor homeostasis and tumorigenesis in the liver. Genes Dev 24, 1718–1730 (2010). [PubMed: 20675406]
58. Lu L, Li Y, Kim SM, Bossuyt W, Liu P, Qiu Q, Wang Y, Halder G, Finegold MJ, Lee JS, Johnson RL, Hippo signaling is a potent in vivo growth and tumor suppressor pathway in the mammalian liver. Proc Natl Acad Sci U S A 107, 1437–1442 (2010). [PubMed: 20080689]

59. Kango-Singh M, Singh A, Regulation of organ size: insights from the Drosophila Hippo signaling pathway. Dev Dyn 238, 1627–1637 (2009). [PubMed: 19517570]
60. Manmadhan S, Ehmer U, Hippo Signaling in the Liver - A Long and Ever-Expanding Story. Front Cell Dev Biol 7, 33 (2019). [PubMed: 30931304]
61. Mooring M, Fowl BH, Lum SZC, Liu Y, Yao K, Softic S, Kirchner R, Bernstein A, Singhi AD, Jay DG, Kahn CR, Camargo FD, Yimlamai D, Hepatocyte Stress Increases Expression of Yes-Associated Protein and Transcriptional Coactivator With PDZ-Binding Motif in Hepatocytes to Promote Parenchymal Inflammation and Fibrosis. Hepatology, (2019).
62. Wang X, Zheng Z, Caviglia JM, Corey KE, Herfel TM, Cai B, Masia R, Chung RT, Lefkowitch JH, Schwabe RF, Tabas I, Hepatocyte TAZ/WWTR1 Promotes Inflammation and Fibrosis in Nonalcoholic Steatohepatitis. Cell Metab 24, 848–862 (2016). [PubMed: 28068223]
63. Moroishi T, Hansen CG, Guan KL, The emerging roles of YAP and TAZ in cancer. Nat Rev Cancer 15, 73–79 (2015). [PubMed: 25592648]
64. Johnson R, Halder G, The two faces of Hippo: targeting the Hippo pathway for regenerative medicine and cancer treatment. Nat Rev Drug Discov 13, 63–79 (2014). [PubMed: 24336504]
65. Xu MZ, Yao TJ, Lee NP, Ng IO, Chan YT, Zender L, Lowe SW, Poon RT, Luk JM, Yes-associated protein is an independent prognostic marker in hepatocellular carcinoma. Cancer 115, 4576–4585 (2009). [PubMed: 19551889]
66. Han SX, Bai E, Jin GH, He CC, Guo XJ, Wang LJ, Li M, Ying X, Zhu Q, Expression and clinical significance of YAP, TAZ, and AREG in hepatocellular carcinoma. J Immunol Res 2014, 261365 (2014). [PubMed: 24860833]
67. Xiao H, Jiang N, Zhou B, Liu Q, Du C, TAZ regulates cell proliferation and epithelial-mesenchymal transition of human hepatocellular carcinoma. Cancer Sci 106, 151–159 (2015). [PubMed: 25495189]
68. Moya IM, Castaldo SA, Van den Mooter L, Soheily S, Sansores-Garcia L, Jacobs J, Mannaerts I, Xie J, Verboven E, Hillen H, Alguero-Nadal A, Karaman R, Van Haele M, Kowalczyk W, De Waegeneer M, Verhulst S, Karras P, van Huffel L, Zender L, Marine JC, Roskams T, Johnson R, Aerts S, van Grunsven LA, Halder G, Peritumoral activation of the Hippo pathway effectors YAP and TAZ suppresses liver cancer in mice. Science 366, 1029–1034 (2019). [PubMed: 31754005]
69. Pepe-Mooney BJ, Dill MT, Alemany A, Ordovas-Montanes J, Matsushita Y, Rao A, Sen A, Miyazaki M, Anakk S, Dawson PA, Ono N, Shalek AK, van Oudenaarden A, Camargo FD, Single-Cell Analysis of the Liver Epithelium Reveals Dynamic Heterogeneity and an Essential Role for YAP in Homeostasis and Regeneration. Cell Stem Cell 25, 23–38 e28 (2019). [PubMed: 31080134]
70. Planas-Paz L, Sun T, Pikiolek M, Cochran NR, Bergling S, Orsini V, Yang Z, Sigoillot F, Jetzer J, Syed M, Neri M, Schuierer S, Morelli L, Hoppe PS, Schwarzer W, Cobos CM, Alford JL, Zhang L, Cuttat R, Waldt A, Carballido-Perrig N, Nigsch F, Kinzel B, Nicholson TB, Yang Y, Mao X, Terracciano LM, Russ C, Reece-Hoyes JS, Gubser Keller C, Sailer AW, Bouwmeester T, Greenbaum LE, Lugus JJ, Cong F, McAllister G, Hoffman GR, Roma G, Tchorz JS, YAP, but Not RSPO-LGR4/5, Signaling in Biliary Epithelial Cells Promotes a Ductular Reaction in Response to Liver Injury. Cell Stem Cell 25, 39–53 e10 (2019). [PubMed: 31080135]
71. Kasumov T, Li L, Li M, Gulshan K, Kirwan JP, Liu X, Previs S, Willard B, Smith JD, McCullough A, Ceramide as a mediator of non-alcoholic Fatty liver disease and associated atherosclerosis. PLoS One 10, e0126910 (2015). [PubMed: 25993337]
72. Kurek K, Piotrowska DM, Wiesiolek-Kurek P, Lukaszuk B, Chabowski A, Gorski J, Zendzian-Piotrowska M, Inhibition of ceramide de novo synthesis reduces liver lipid accumulation in rats with nonalcoholic fatty liver disease. Liver Int 34, 1074–1083 (2014). [PubMed: 24106929]
73. Xia JY, Holland WL, Kusminski CM, Sun K, Sharma AX, Pearson MJ, Sifuentes AJ, McDonald JG, Gordillo R, Scherer PE, Targeted Induction of Ceramide Degradation Leads to Improved Systemic Metabolism and Reduced Hepatic Steatosis. Cell Metab 22, 266–278 (2015). [PubMed: 26190650]
74. Chaurasia B, Tippetts TS, Mayoral Monibas R, Liu J, Li Y, Wang L, Wilkerson JL, Sweeney CR, Pereira RF, Sumida DH, Maschek JA, Cox JE, Kaddai V, Lancaster GI, Siddique MM, Poss A, Pearson M, Satapati S, Zhou H, McLaren DG, Previs SF, Chen Y, Qian Y, Petrov A, Wu M, Shen X, Yao J, Nunes CN, Howard AD, Wang L, Erion MD, Rutter J, Holland WL, Kelley DE,

Summers SA, Targeting a ceramide double bond improves insulin resistance and hepatic steatosis. Science 365, 386–392 (2019). [PubMed: 31273070]

75. Ichi I, Nakahara K, Fujii K, Iida C, Miyashita Y, Kojo S, Increase of ceramide in the liver and plasma after carbon tetrachloride intoxication in the rat. J Nutr Sci Vitaminol (Tokyo) 53, 53–56 (2007). [PubMed: 17484380]
76. Xia JY, Morley TS, Scherer PE, The adipokine/ceramide axis: key aspects of insulin sensitization. Biochimie 96, 130–139 (2014). [PubMed: 23969158]
77. Yetukuri L, Katajamaa M, Medina-Gomez G, Seppanen-Laakso T, Vidal-Puig A, Oresic M, Bioinformatics strategies for lipidomics analysis: characterization of obesity related hepatic steatosis. BMC Syst Biol 1, 12 (2007). [PubMed: 17408502]
78. Luukkonen PK, Zhou Y, Sadevirta S, Leivonen M, Arola J, Oresic M, Hyotylainen T, Yki-Jarvinen H, Hepatic ceramides dissociate steatosis and insulin resistance in patients with non-alcoholic fatty liver disease. J Hepatol 64, 1167–1175 (2016). [PubMed: 26780287]
79. Meikle PJ, Wong G, Barlow CK, Weir JM, Greeve MA, MacIntosh GL, Almasy L, Comuzzie AG, Mahaney MC, Kowalczyk A, Haviv I, Grantham N, Magliano DJ, Jowett JB, Zimmet P, Curran JE, Blangero J, Shaw J, Plasma lipid profiling shows similar associations with prediabetes and type 2 diabetes. PLoS One 8, e74341 (2013). [PubMed: 24086336]
80. Lemaitre RN, Yu C, Hoofnagle A, Hari N, Jensen PN, Fretts AM, Umans JG, Howard BV, Sitlani CM, Siscovick DS, King IB, Sotoodehnia N, McKnight B, Circulating Sphingolipids, Insulin, HOMA-IR, and HOMA-B: The Strong Heart Family Study. Diabetes 67, 1663–1672 (2018). [PubMed: 29588286]
81. Angulo P, Kleiner DE, Dam-Larsen S, Adams LA, Bjornsson ES, Charatcharoenwitthaya P, Mills PR, Keach JC, Lafferty HD, Stahler A, Haflidadottir S, Bendtsen F, Liver Fibrosis, but No Other Histologic Features, Is Associated With Long-term Outcomes of Patients With Nonalcoholic Fatty Liver Disease. Gastroenterology 149, 389–397 e310 (2015). [PubMed: 25935633]
82. Liu X, Yue S, Li C, Yang L, You H, Li L, Essential roles of sphingosine 1-phosphate receptor types 1 and 3 in human hepatic stellate cells motility and activation. J Cell Physiol 226, 2370–2377 (2011). [PubMed: 21660960]
83. Li C, Zheng S, You H, Liu X, Lin M, Yang L, Li L, Sphingosine 1-phosphate (S1P)/S1P receptors are involved in human liver fibrosis by action on hepatic myofibroblasts motility. J Hepatol 54, 1205–1213 (2011). [PubMed: 21145832]
84. Ikeda H, Yatomi Y, Yanase M, Satoh H, Maekawa H, Ogata I, Ozaki Y, Takuwa Y, Mochida S, Fujiwara K, Biological activities of novel lipid mediator sphingosine 1-phosphate in rat hepatic stellate cells. Am J Physiol Gastrointest Liver Physiol 279, G304–310 (2000). [PubMed: 10915638]
85. Finch-Edmondson ML, Strauss RP, Passman AM, Sudol M, Yeoh GC, Callus BA, TAZ Protein Accumulation Is Negatively Regulated by YAP Abundance in Mammalian Cells. J Biol Chem 290, 27928–27938 (2015). [PubMed: 26432639]
86. Lavado A, He Y, Pare J, Neale G, Olson EN, Giovannini M, Cao X, Tumor suppressor Nf2 limits expansion of the neural progenitor pool by inhibiting Yap/Taz transcriptional coactivators. Development 140, 3323–3334 (2013). [PubMed: 23863479]
87. Eliyahu E, Shtraizent N, Shalgi R, Schuchman EH, Construction of conditional acid ceramidase knockout mice and in vivo effects on oocyte development and fertility. Cell Physiol Biochem 30, 735–748 (2012). [PubMed: 22854249]
88. Henderson NC, Arnold TD, Katamura Y, Giacomini MM, Rodriguez JD, McCarty JH, Pellicoro A, Raschperger E, Betsholtz C, Ruminski PG, Griggs DW, Prinsen MJ, Maher JJ, Iredale JP, Lacy-Hulbert A, Adams RH, Sheppard D, Targeting of alphav integrin identifies a core molecular pathway that regulates fibrosis in several organs. Nat Med 19, 1617–1624 (2013). [PubMed: 24216753]
89. Mederacke I, Dapito DH, Affo S, Uchinami H, Schwabe RF, High-yield and high-purity isolation of hepatic stellate cells from normal and fibrotic mouse livers. Nat Protoc 10, 305–315 (2015). [PubMed: 25612230]

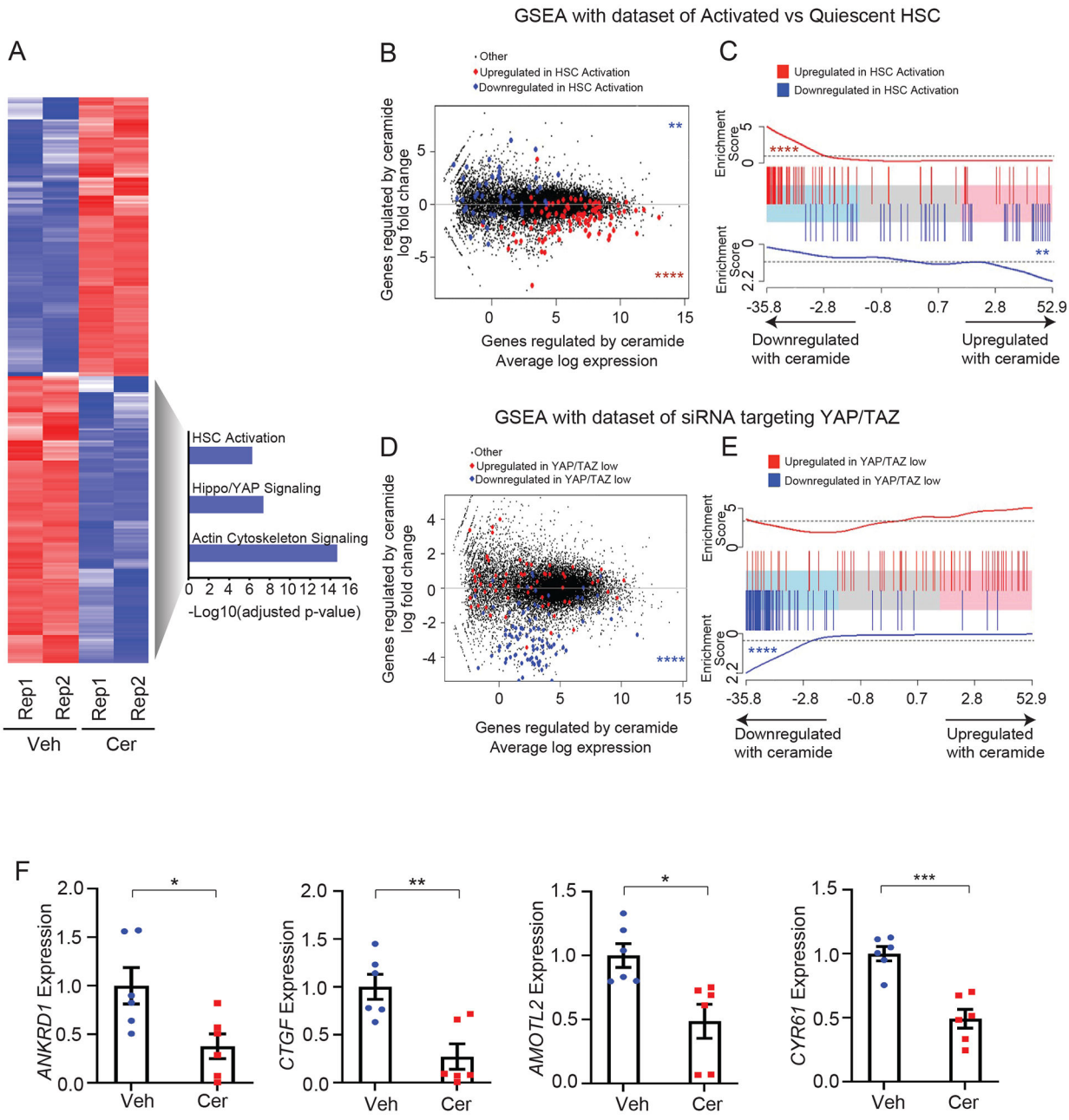

Fig. 1. Ceramide regulates the Hippo signaling pathway in human hepatic stellate cells.

(A) Heatmap of genes profiled by RNASeq induced (red) or repressed (blue) at ≥1.5-log fold change (false discovery rate (FDR) < 0.05) in HSCs treated with ceramide-C6 (25 μM, Cer) compared to ethanol vehicle (Veh). Canonical pathways downregulated by ceramide are shown to the right. **(B)** The genes most up- (red, n=97) and downregulated (blue, n=48) in activated as compared to quiescent human HSCs (33) overlaid on the mean difference plot for all genes (additional genes: black) profiled in HSCs treated with ceramide versus vehicle (downregulated below x-axis). Genes downregulated with HSC activation are enriched amongst genes upregulated by ceramide (blue points mostly above the x-axis, GSEA $P <$ 0.01). Genes upregulated with HSC activation are enriched amongst genes downregulated by

ceramide (red points mostly below the x-axis, GSEA $P < 0.0001$). **(C)** A barcode plot in which the vertical lines represent the same genes most up- (red) and downregulated (blue) after HSC activation positioned by rank amongst all genes in ceramide-treated HSCs ordered from least to most upregulated with ceramide (light blue to pink in the underlying color bar). Red lines are clustered to the left and the enrichment score line plot below crosses the dashed line once, showing enrichment of genes upregulated with HSC activation amongst genes downregulated by ceramide. Blue lines are clustered to the right, showing enrichment of genes downregulated with HSC activation amongst genes upregulated by ceramide. Similar **(D)** mean difference and **(E)** barcode plots as in (**B** and **C**) but using genes most up- (red, n=61) and downregulated (blue, n=92) after YAP/TAZ depletion by siRNAs in HepG2 cells (35) at FDR < 0.05 for the comparison to genes up- and downregulated with ceramide treatment in HSCs. Genes downregulated with YAP/TAZ depletion are enriched amongst genes downregulated by ceramide ($P < 0.0001$). **(F)** qRT-PCR quantified expression (mean ± s.e.m.) of the indicated genes after treatment with ethanol vehicle or ceramide-C6 (25 μM) for 48 hours, compared using unpaired two-sided student t-tests. Samples are normalized to *GAPDH.* $n = 6$ biologically independent samples and results are representative of 3 independent experiments. Data are expressed as mean ± s.e.m. For GSEA, statistical analysis was performed with CAMERA. (* $P < 0.05$; ** $P < 0.01$, *** $P < 0.001$, **** $P < 0.0001$).

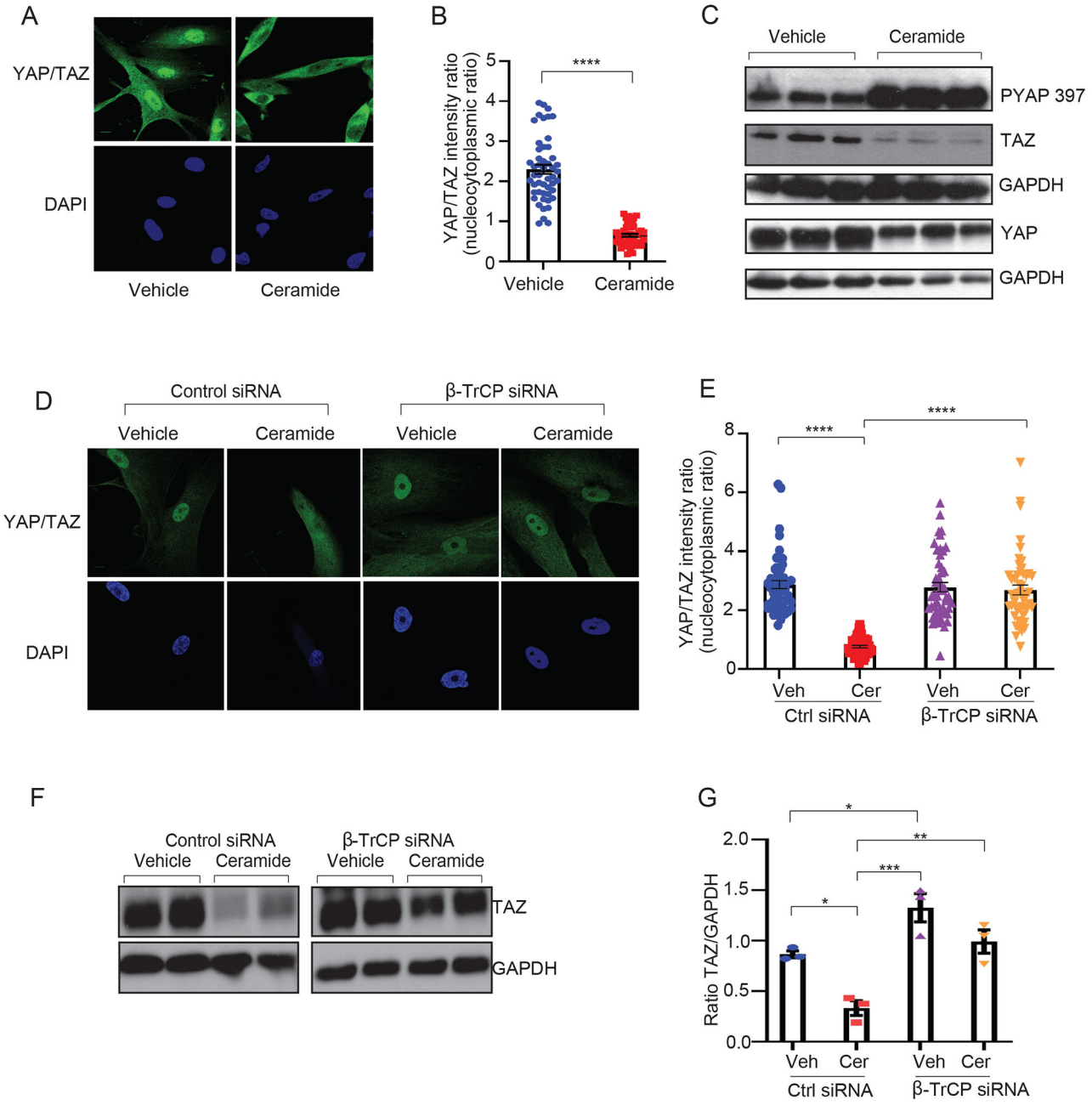

Fig. 2. Ceramide inhibits YAP/TAZ nuclear localization and promotes β-TrCP-mediated proteasomal degradation of YAP/TAZ.

(A, B) Human HSCs were treated with ethanol vehicle (left) or ceramide-C6 (25 μM, right) for 6 hours. **(A)** Immunofluorescence (IF) with anti-YAP/TAZ antibody (top, green) and DAPI (bottom, blue). Scale bar: 10 μm. **(B)** Quantification of YAP/TAZ mean fluorescence nucleocytoplasmic intensity ratio (N/C ratio) was performed for 50 cells per condition. **(C)** Expression of Phospho-YAP (Ser397), TAZ, and GAPDH were quantified by Western blot from HSCs treated with ethanol vehicle (left) or ceramide-C6 (25 μM, right) for 6 hours. Expression of YAP and GAPDH were quantified by Western blot after treatment for 72 hours. Cropped gel images are shown. **(D-G)** HSCs were transfected with a nontargeting

(control) siRNA or siRNA targeting *BTRC* (β-TrCP). After 48 hours, cells were treated with ethanol vehicle or ceramide-C6 (25 μM) for 6 hours. **(D)** IF with anti-YAP/TAZ antibody (top, green) and DAPI (bottom, blue). Scale bar: 10 μm. (E) Quantification of IF staining showing YAP/TAZ N/C ratio measured in 50 cells for each condition. **(F)** Expression of TAZ and GAPDH were quantified by Western blot. Cropped gel images are shown. **(G)** The ratio of TAZ to GAPDH is shown. $n = 3$ biologically independent samples and results are representative of 3 independent experiments. Data are expressed as mean ± s.e.m. Subsequent statistical analysis was performed with unpaired two-sided student t-tests or one-way ANOVA with Tukey's method for multiple comparisons. (* $P < 0.05$; ** $P < 0.01$, *** $P < 0.001$, **** $P < 0.0001$).

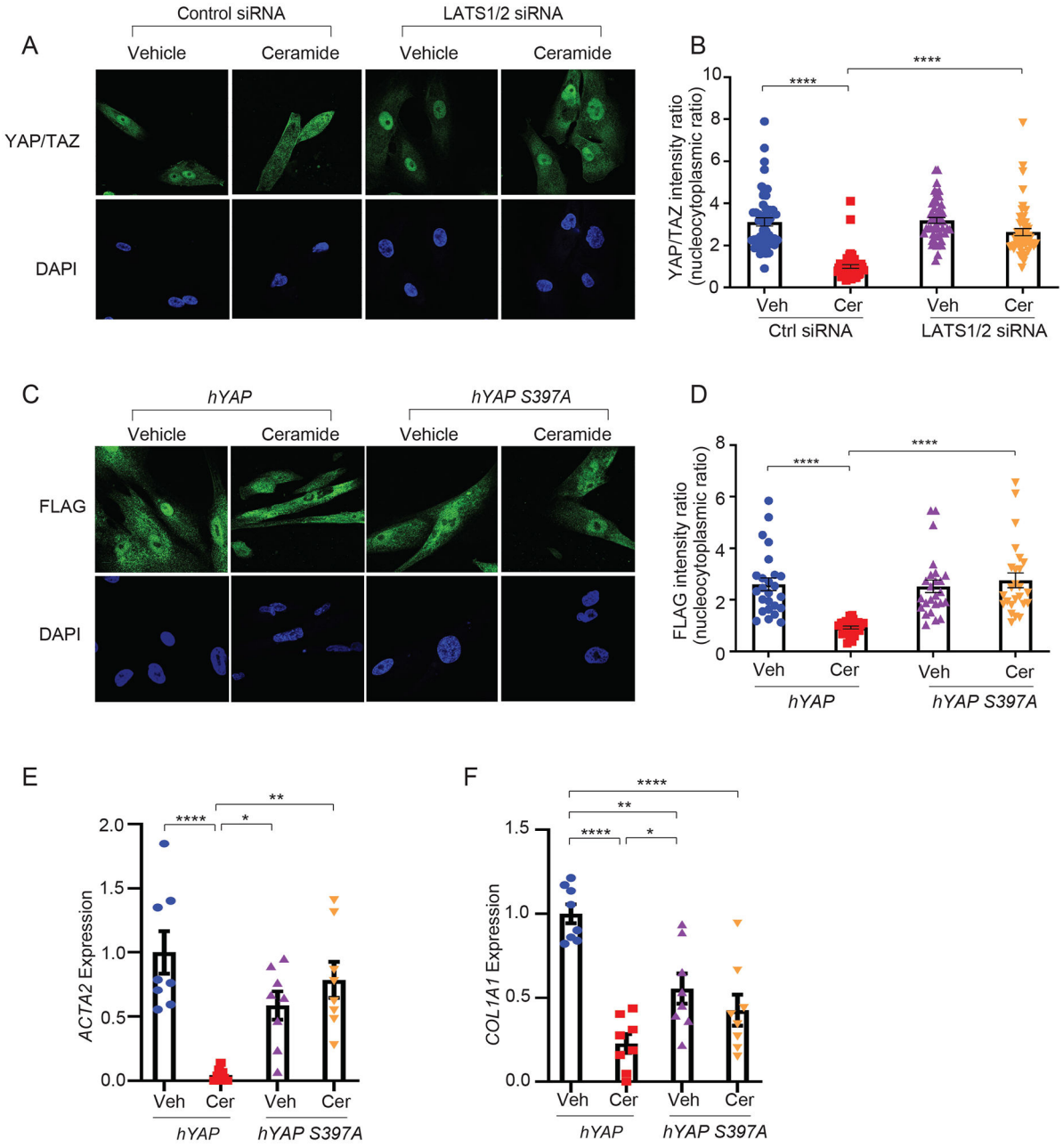

Fig. 3. Ceramide regulation of YAP/TAZ localization and HSC activation is mediated by LATS1/2.

(A, B) HSCs were transfected with nontargeting siRNAs (control) or siRNAs targeting LATS1 and LATS2. After 72 hours, cells were treated with ethanol vehicle or ceramide-C6 (25 μM) for 6 hours. **(A)** IF with anti-YAP/TAZ antibody (top, green) and DAPI (bottom, blue). Scale bar: 10 μm. **(B)** Quantification of YAP/TAZ N/C ratio was performed for 50 cells per condition. **(C-F)** HSCs were nucleofected with FLAG-tagged *hYAP* or $hYAP^{S397A}$. After 24 hours, cells were treated with ethanol vehicle or ceramide-C6 (25 μM) for 6 hours. **(C)** IF with anti-FLAG antibody (top, green) and DAPI (bottom, blue). Scale bar: 10 μm. **(D)** Quantification of FLAG N/C ratio was performed for 50 cells per condition. **(E, F)** qRT-

PCR was performed to quantify expression of the indicated genes. Samples were normalized to *GAPDH*. $n = 8$ biologically independent samples and results are representative of 3 independent experiments. Data are expressed as mean ± s.e.m. Subsequent statistical analysis was performed with one-way ANOVA with Tukey's method for multiple comparisons. (* $P < 0.05$, ** $P < 0.01$, **** $P < 0.0001$).

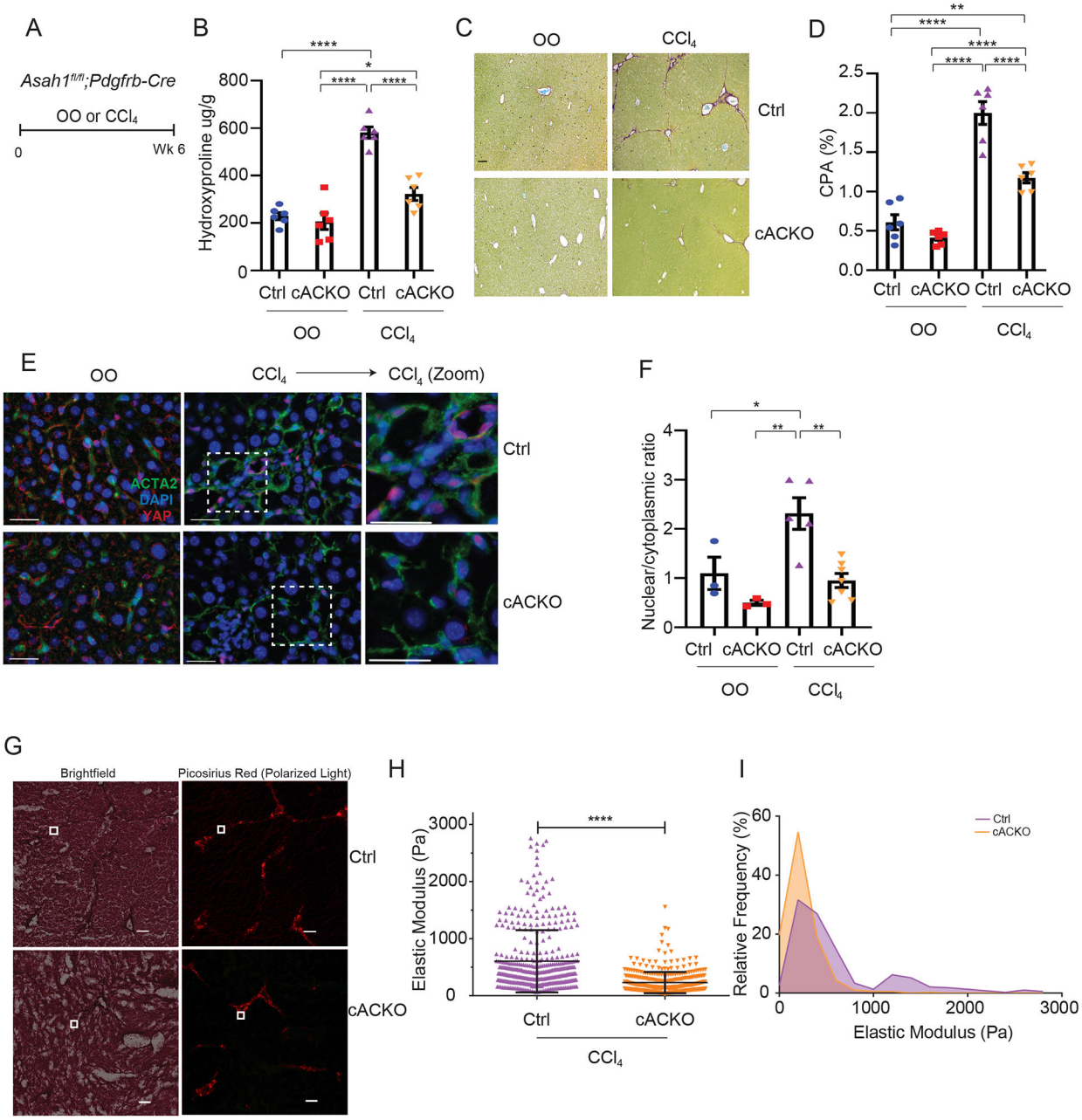

Fig. 4. aCDase deficiency in HSCs reduces CCl_4-induced liver fibrosis in mice.

(A) Olive oil (OO) or CCl_4 was administered three times a week by IP injection for 6 weeks to control (Ctrl) and cACKO mice. **(B)** Hepatic hydroxyproline was measured in mice from each treatment group. **(C)** Representative images of liver tissues with Sirius-red staining. Scale bar: 100 μm. **(D)** Morphometric assessment of the collagen proportional area (CPA) on Sirius-red stained slides. *n=6* in each group. **(E)** Representative IF images of liver tissues for α-SMA (*ACTA2*, green), DAPI (blue), and YAP (red). Scale bar: 30 μm. **(F)** Quantification of YAP N/C ratio was performed for at least 200 α-SMA positive cells per mouse. *n=3* Ctrl +OO, *n=3* cACKO+ OO, *n=5* Ctrl+CCl_4, *n=7* cACKO+CCl_4. **(G)** Images of liver tissues stained with picrosirius red and Weigert's hematoxylin viewed under brightfield (left) and

orthogonal polarizing filters (right). Scale bar: 100 μm. White box (50x50 μm) area is representative of an area where an AFM Force Map indentation of 8x8 points was performed. **(H)** Scatter plot of elastic modulus (a measure of stiffness) values in Pascals (Pa) measured by AFM in tissue sections of livers of Ctrl and cACKO mice treated with CCl_4 (n = 3 mice per group and 2 tissue sections from each mouse, 3 to 4 50 x 50 μm regions per section, 64 indentations per map). Mean ± SD. **(I)** Histograms of elastic modulus values from **(F)** from livers of Ctrl and cACKO mice treated with CCl_4. Data are expressed as mean ± s.e.m unless indicated and results are representative of 2 independent experiments. Subsequent statistical analysis was performed with one-way ANOVA with Tukey's method for multiple comparisons or nonparametric two-sided Mann-Whitney test. (* $P < 0.05$; ** $P < 0.01$, **** $P < 0.0001$).

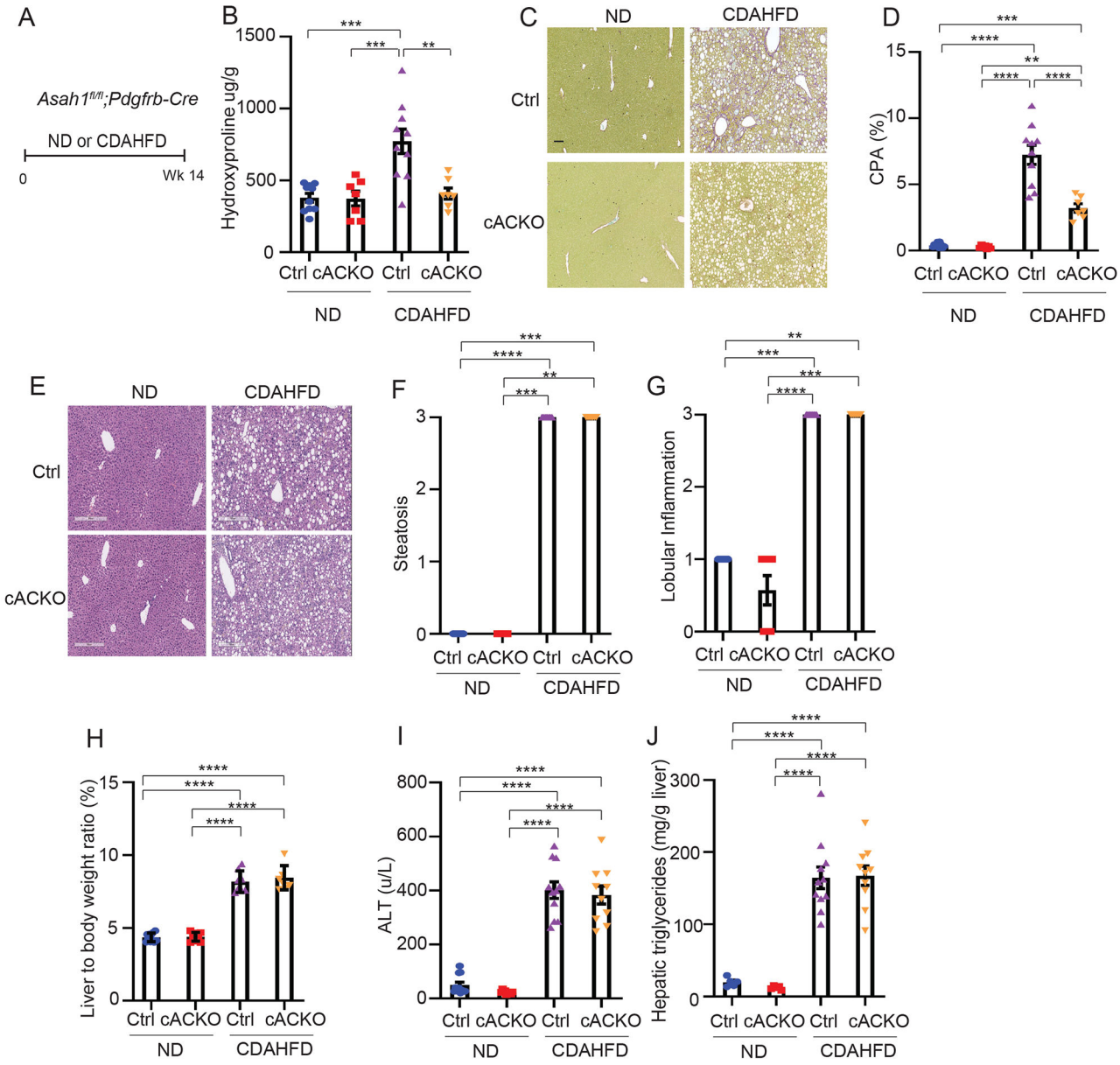

Fig. 5. aCDase deficiency in HSCs reduces NASH fibrosis in mice.

(A) Ctrl or cACKO mice were fed normal diet (ND) or choline-deficient, L-amino acid-defined, high-fat diet (CDAHFD) for 14 weeks. **(B)** Hepatic hydroxyproline was measured in mice from each treatment group. **(C)** Representative images of liver sections with Sirius-red staining. Scale bar: 100 μm. **(D)** Morphometric assessment of CPA on Sirius-red stained slides. *n=10* Ctrl+ND, *n=7* cACKO+ND, *n=10* Ctrl+CDAHFD, *n=7* cACKO+CDAHFD. **(E)** Representative images of liver sections with H&E staining. Scale bar: 300 μm. **(F, G)** Histologic evaluation of steatosis and lobular inflammation. *n=11* in Ctrl+ND, *n=7* cACKO +ND, *n=10* Ctrl+CDAHFD, *n=7* cACKO+CDAHFD. **(H)** Liver weight to body weight ratio. *n=11* in Ctrl+ND, *n=10* cACKO+ND, *n=8* Ctrl+CDAHFD, *n=8* cACKO+CDAHFD. **(I)** Serum alanine aminotransferase (ALT). *n=11* Ctrl+ND, *n=10* cACKO+ND, *n=11* Ctrl+ CDAHFD, *n=10* cACKO+CDAHFD. **(J)** Quantitative hepatic triglycerides. *n=5* Ctrl+ND,

n=5 cACKO+ND, *n=11* Ctrl+CDAHFD, *n=10* cACKO+CDAHFD. Data are expressed as mean ± s.e.m and results are representative of 2 independent experiments. Subsequent statistical analysis was performed with one-way ANOVA with Tukey's method for multiple comparisons or Kruskal-Wallis test with Dunn's multiple comparisons test. (** $P < 0.01$, *** $P < 0.001$, **** $P < 0.0001$).

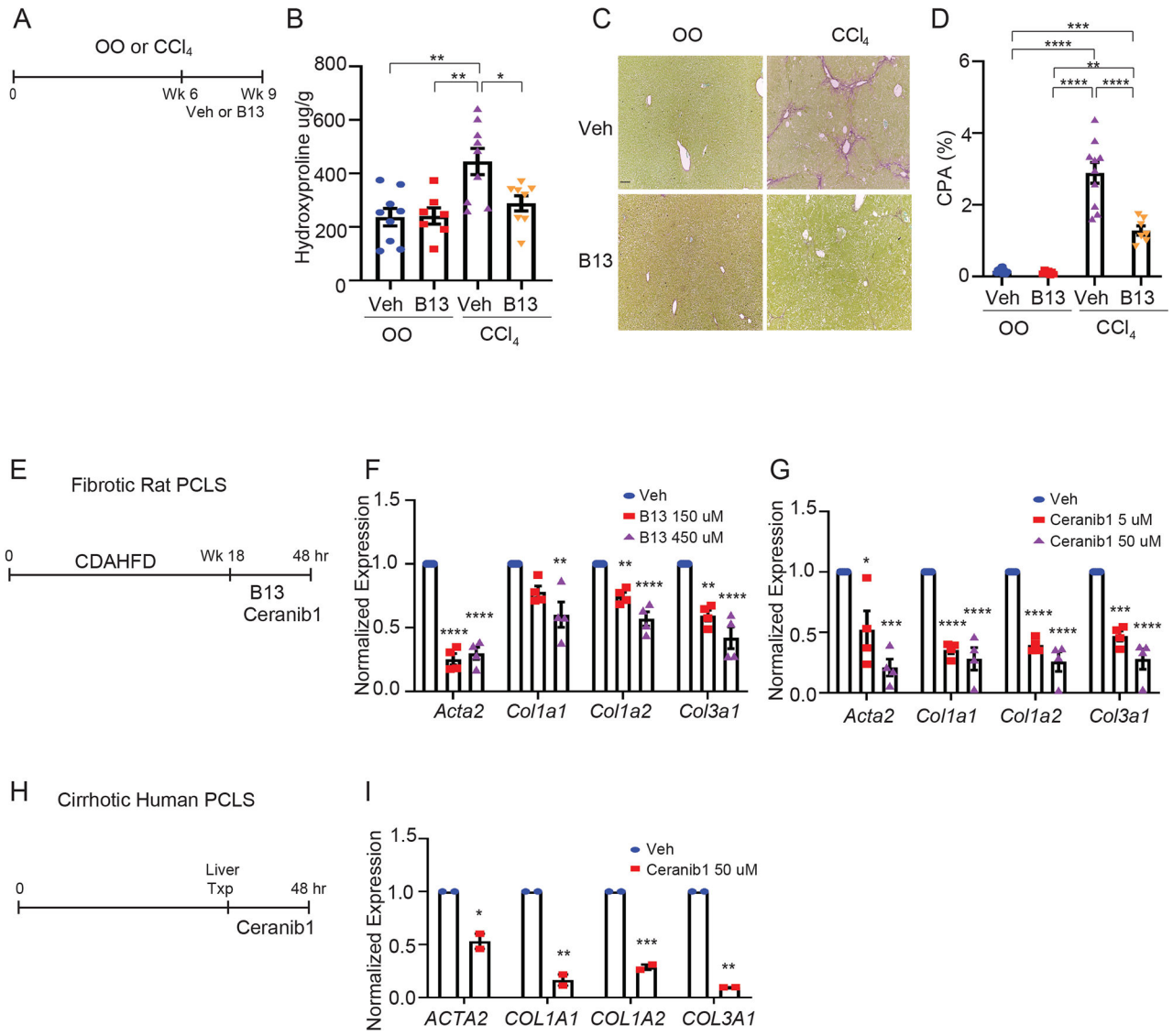

Fig. 6. aCDase inhibition ameliorates liver fibrosis.

(A) C57BL/6J mice received olive oil (OO) or CCl_4 three times a week by IP injection for a total of 9 weeks. B13 (50 mg/kg) or vehicle (Veh) were concomitantly administered by IP injection five times per week for the last 3 weeks of OO or CCl_4 treatment. **(B)** Hepatic hydroxyproline was measured in mice from each treatment group. *n=9* OO+Veh, *n=7* OO +B13, *n=9* CCl_4+Veh, and *n=8* CCl_4+B13.**(C)** Representative images of liver sections with Sirius-red staining. Scale bar: 100 μm. **(D)** Morphometric assessment of CPA on Sirius-red stained slides. *n=9* OO+Veh, *n=7* OO+B13, *n=9* CCl_4+Veh, and *n=7* CCl_4+B13. **(E)** Rats were fed CDAHFD for 18 weeks, and precision cut liver slices (PCLS) were prepared. Rat PCLS were treated with ethanol vehicle (Veh), B13 150 μM, or B13 450 μM; or DMSO vehicle (Veh), Ceranib1 5 μM, or Ceranib1 50 μM for 48 hours. **(F, G)** Gene expression assessment using nCounter technology was performed to quantify expression of the indicated genes. mRNA counts were normalized to housekeeping genes (*Hprt1, Polr1b, Rplp0, Srfs4, Ubc* and *Gusb*), and expression relative to the appropriate vehicle control

group from the same rat liver is reported. $n = 4$ rats per treatment group, and three slices from each rat were included in each treatment group. **(H)** PCLS were prepared from the livers of 2 patients with cirrhosis undergoing liver transplantation, one with alcoholic cirrhosis and one with primary biliary cirrhosis. Human cirrhotic PCLS were treated with DMSO vehicle (Veh) or Ceranib1 50 uM for 48 hours. **(I)** Gene expression assessment using nCounter technology was performed to quantify expression of the indicated genes. mRNA counts were normalized to housekeeping genes (*HPRT1, POLR1B, RPLP0, SRFS4, UBC*, and *GUSB*), and expression relative to the appropriate vehicle control group from the same patient is reported. $n = 2$ patients per treatment group, and three slices from each patient were included in each treatment group. Data are expressed as mean ± s.e.m. Subsequent statistical analysis was performed with unpaired two-sided student t-tests or one-way ANOVA with Tukey's method for multiple comparisons. (* $P < 0.05$; ** $P < 0.01$, *** $P < 0.001$, **** $P < 0.0001$).

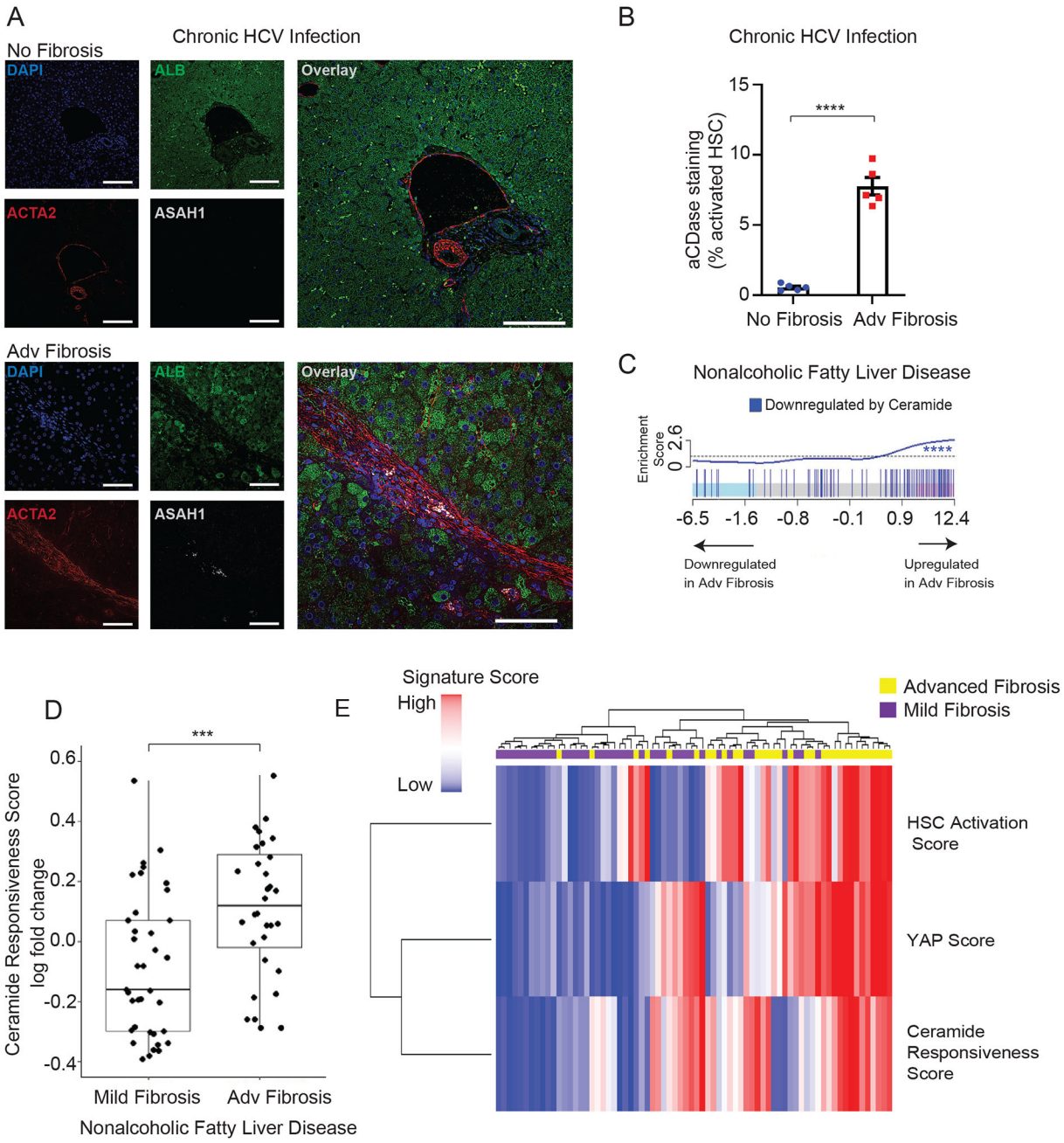

Fig. 7. aCDase and the ceramide responsiveness score are increased in patients with advanced liver fibrosis.

(A) Representative IF images for albumin (*ALB*), α-SMA (*ACTA2*), aCDase (*ASAH1*), and DAPI in liver sections from patients with chronic hepatitis C virus (HCV) infection and no fibrosis (top) and those with chronic HCV and advanced fibrosis (bottom). Scale bar: 150 μm (top), 50 μm (bottom)μm. **(B)** Quantification of aCDase staining among activated HSCs. $n = 5$ in no fibrosis and $n = 5$ in advanced fibrosis. **(C)** The barcode plot represents the 100 genes most downregulated by ceramide as blue vertical lines positioned by rank amongst all genes profiled by microarray in an NAFLD dataset ordered by genes most downregulated to most upregulated by log fold change in participants with advanced fibrosis (stage 3-4, n=32)

as compared to mild fibrosis (Stage 0-1, n=40) (54). Blue lines are clustered to the right and the enrichment score line plot below crosses the dashed line once, indicating enrichment of genes downregulated by ceramide amongst genes upregulated in advanced fibrosis (GSEA P <0.0001). **(D)** A ceramide responsiveness score was generated by combining the 100 genes most downregulated by ceramide treatment into one metric using gene set variation analysis (GSVA). The boxplots compare this score between NAFLD patients with mild fibrosis (left) and advanced fibrosis (right). (**E**) Heatmap of gene signature scores for the specified biologic pathways generated in GSVA (rows) clustered by participants in the NAFLD dataset (columns), with high signature expression in red and low in blue. Participants with advanced and mild fibrosis are indicated by yellow and purple, respectively, in the above color bar. Clustering is by Euclidean distance with average linkage. Statistical analysis was performed with unpaired two-sided student t-tests or with CAMERA for GSEA. (*** P < 0.001, **** P < 0.0001).